



The weakening AMOC under extreme climate change

Gaurav Madan¹ · Ada Gjermundsen^{1,2} · Silje C. Iversen³ · Joseph H. LaCasce¹

Received: 27 March 2023 / Accepted: 8 September 2023 / Published online: 6 October 2023
© The Author(s) 2023

Abstract

Changes in the Atlantic Meridional Overturning Circulation (AMOC) in the quadrupled CO₂ experiments conducted under the sixth Coupled Model Intercomparison Project (CMIP6) are examined. Increased CO₂ triggers extensive Arctic warming, causing widespread melting of sea ice. The resulting freshwater spreads southward, first from the Labrador Sea and then the Nordic Seas, and proceeds along the eastern coast of North America. The freshwater enters the subpolar gyre north of the separated Gulf Stream, the North Atlantic Current. This decreases the density gradient across the current and the current weakens in response, reducing the inflow to the deepwater production regions. The AMOC cell weakens in tandem, first near the North Atlantic Current and then spreading to higher and lower latitudes. This contrasts with the common perception that freshwater caps the convection regions, stifling deepwater production; rather, it is the inflow to the subpolar gyre that is suppressed. Changes in surface temperature have a much weaker effect, and there are no consistent changes in local or remote wind forcing among the models. Thus an increase in freshwater discharge, primarily from the Labrador Sea, is the precursor to AMOC weakening in these simulations.

Keywords AMOC · Gulf stream · CMIP6 · IPCC · Climate change

1 Introduction

The large-scale ocean circulation transports heat, nutrients, freshwater, and carbon around the globe. In the Northern Hemisphere alone, 1.5–2 PW (1 PW = 10¹⁵ W) of heat

is transported meridionally in the ocean (Ganachaud and Wunsch 2003). An essential part of this occurs in the Atlantic Ocean (Trenberth et al. 2001), in the so-called Atlantic Meridional Overturning Circulation (AMOC). AMOC has distinct branches and a complex three dimensional structure, with warm shallow waters entering and sinking in the Labrador and Nordic Seas, recirculating in the Arctic and then exiting the Denmark Straits at depth to supply the North Atlantic Deep Water (NADW) (Johnson et al. 2019; Bower et al. 2019).

AMOC is often represented as a two-dimensional circulation in latitude and depth (Broecker 1991; Wright and Stocker 1991; Schmitz 1996; Cessi 2019). This is as is commonly done in the atmosphere; the three dimensional meridional circulation is made two dimensional following zonal integration of the velocities. The resulting oceanic cells—primarily the AMOC and Antarctic Bottom Water (AABW)—are a simple means of comparing the response across models. But the integration obscures the 3D structure of the flow, with its western boundary currents and horizontal recirculations. The latter, for example, can extend the meridional pathways in both the upper and lower limbs of the AMOC, as fluid parcels may be delayed for years before

Ada Gjermundsen, Silje C. Iversen and Joseph. H. LaCasce contributed equally to this work.

✉ Gaurav Madan
gaurav.madan@geo.uio.no

Ada Gjermundsen
adag@met.no

Silje C. Iversen
silje.c.iversen@uit.no

Joseph H. LaCasce
j.h.lacasse@geo.uio.no

¹ Section for Meteorology and Ocean Sciences, University of Oslo, Blindernveien 31, 0371 Oslo, Norway

² Division for Climate Modelling and Air Pollution, Norwegian Meteorological Institute, Henrik Mohns plass 1, 0313 Oslo, Norway

³ Department of Physics and Technology, UiT The Arctic University of Norway, P.O. Box 6050 Langnes, 9037 Tromsø, Norway

moving northward. This could greatly increase their net exposure to the atmosphere (Bower et al. 2019).

AMOC is not stationary, but varies on a range of time scales, from weekly to centennial (Bryden et al. 2005; Delworth and Mann 2000; Knight 2005; Jackson et al. 2015; Lopez et al. 2016; Zhang et al. 2019). AMOC is predicted to weaken in the warming climate as well. The observational evidence for this is equivocal, as the records are relatively short; while data from the Rapid Climate Change (RAPID) array at 26.5°N in the North Atlantic indicates some weakening (Häkkinen and Rhines 2004; Bryden et al. 2005; McCarthy et al. 2012; Robson et al. 2013; Smeed 2014, 2018), evidence from basin-wide observations in the North and South Atlantic suggest that there has been no significant change since 2012 (Lozier et al. 2017, 2019; Fu et al. 2020; Li et al. 2021; Caínzos et al. 2022). Predictions of AMOC weakening are based instead on climate model simulations (Cheng et al. 2013; Weaver et al. 2012; Fox-Kemper et al. 2021). These indicate a 24–39% decline by the end of the twentyfirst century, with more weakening with larger increases in greenhouse gas (GHG) emissions (Lin and Zhang 2004; Gregory 2005; Schmittner et al. 2005; Drijfhout and Hazeleger 2007; Weaver et al. 2012; Cheng et al. 2013; Reintges et al. 2017; Menary et al. 2020; Fox-Kemper et al. 2021; Weijer et al. 2020).

Despite consistent indications from model simulations, there is a lack of consensus on the driving mechanisms for the weakening. These have been linked to changes in wind forcing, buoyancy forcing or a combination of the two. Changes in the local zonal wind stress affect the AMOC strength on sub-decadal timescales (Jayne and Marotzke 2001; Hirschi et al. 2003, 2007; Kuhlbrodt et al. 2007; Kanzow et al. 2010; Polo et al. 2014; Yeager 2015). AMOC has also been linked to the wind-driven Ekman transport from the Southern Ocean, which is of a similar magnitude (20 Sv) (Toggweiler and Samuels 1995, 1998; Wunsch 2004; Kuhlbrodt et al. 2007; Cessi 2019). Indeed, there is evidence in some models that a reduction in AMOC could be balanced by increased overturning in the Southern Ocean, due to increased wind forcing there. This “bipolar seesaw” effect has been invoked to explain ice core records from Greenland and Antarctica (Stocker and Johnsen 2003).

Buoyancy forcing, from changes in surface heating or evaporation/precipitation, has been implicated in longer term variations (Yeager and Danabasoglu 2014). Anomalous surface heat fluxes have been shown to increase upper-ocean stratification in the subpolar North Atlantic, affecting deep water formation (Dixon et al. 1999; Schmittner et al. 2005; Gregory 2005; Stouffer et al. 2006; Weaver et al. 2007; Liu et al. 2014, 2017, 2019; Gregory et al. 2016; Maroon et al. 2018). Other studies suggest that subsurface warming weakens overturning (Haskins et al. 2020; Levang and Schmitt 2020a; Bonan et al. 2022).

More often though, AMOC changes are associated with freshwater fluxes from melting sea ice and glaciers (Manabe and Stouffer 1995; Ganopolski and Rahmstorf 2001; Rind et al. 2001; Vellinga and Wood 2002; Knutti et al. 2004; Stouffer et al. 2006; Weijer et al. 2019; He and Clark 2022). Indeed, “hosing” experiments, in which a large volume of freshwater is introduced suddenly in the subpolar gyre, exhibit drastic AMOC weakening. The response however is strongly model dependent (Proshutinsky et al. 2015; Rahmstorf et al. 2015; Bakker 2016).

Changes in surface temperature and salinity often occur in tandem. Enhanced heating at high latitudes reduces surface densities but also melts sea ice, further increasing buoyancy (Cheng et al. 2013; Liu et al. 2019). The resulting increase in surface buoyancy in the subpolar gyre is believed to suppress deepwater formation. It has been suggested that this could tip the system to a new overturning state, following idealized models such as Stommel’s (1961). However the importance of deep convection for the overturning is disputed. Some argue that AMOC is not “pushed” by convection but rather “pulled” by mixing in the ocean interior (Wunsch 2002; Visbeck 2007). Others contend that surface buoyancy forcing itself is the primary driver, by inducing a meridional density gradient (de Verdière 1988; Gjermundsen and LaCasce 2017; Gjermundsen et al. 2018).

Hereafter, we examine AMOC changes in one of the most extreme of the CMIP6 simulations, in which CO₂ is suddenly quadrupled. While unrealistic, the abrupt transition facilitates diagnosing the response. We find that wind forcing, both local and in the Southern Ocean, does not change in a consistent manner between the models and is not correlated with AMOC weakening. Rather, AMOC decline is strongly correlated with the density gradient across the separated Gulf Stream, the North Atlantic Current (NAC). The gradient is weakened by freshwater fluxes from melted sea ice which enter the subpolar gyre from the western boundary. The weakened gradient yields a weaker baroclinic shear, following the thermal wind relation. The AMOC, which derives from the zonal and vertical integrals of the meridional velocity, decreases proportionally.

The model simulations are discussed in Sect. 2. AMOC weakening and its dependence on wind- and buoyancy-forcing is examined in Sect. 3. The results are discussed and summarized in Sect. 4.

2 Materials and methods

We employ coupled climate simulations from the Coupled Model Intercomparison Project Phase 6 (CMIP6) project (Eyring et al. 2016). The focus will be on the abrupt-4xCO₂ experiment (“4xCO₂” hereafter), in which the CO₂ concentration is abruptly quadrupled and held fixed thereafter,

keeping all other external forcings the same. The results will be compared to those from the pre-industrial control run (“control”) with no increase in greenhouse gas emissions. The 4xCO₂ run is a standard test case in the CMIP ensemble. For comparison, a 1% increase of CO₂ per year would yield a quadrupling in 139 years. We use 35 different GCM simulations for comparison (refer Table 1 in “Appendix”).

The AMOC streamfunction is calculated by integrating the meridional velocity, v_o , zonally between the continental boundaries from x_w to x_e at a given latitude and with depth, thus:

$$\Psi(y, z) = \int_z^0 \int_{x_w}^{x_e} v_o(x, y, z') dx dz' \tag{1}$$

The streamfunction is calculated in each of the basins, i.e., Atlantic-Arctic, Indian-Pacific, and globally. Note that while calculating the streamfunction as a function of density yields a better indication of the Lagrangian transport, e.g. (Nycander et al. 2007; Johnson et al. 2019), the z-coordinate version here is more conducive to the present analysis.

When examining the response to surface buoyancy forcing, it is useful to separate the density changes into those due to temperature and to salinity (e.g. Dai 2022):

$$\Delta\rho(S, T, P) = \frac{\partial\rho(S, T, P)}{\partial T} \Delta T + \frac{\partial\rho(S, T, P)}{\partial S} \Delta S \tag{2}$$

where ρ is density at temperature T , salinity S and pressure P . We will be primarily concerned with the surface density, for which $P = 0$. To evaluate the derivatives, we use UNESCO’s equation of state for seawater (Fofonoff and Millard 1983). The derivatives are evaluated from the 50-year-mean of the control run, and the changes in temperature and salinity, ΔT and ΔS , calculated from differences between the 4xCO₂ and control runs after a selected time, here 100 years.

Changes in the surface density affect the vertical shear of the horizontal velocities via the thermal wind relation. Under the Boussinesq approximation, the relation for the zonal velocity is:

$$\frac{\partial u}{\partial z} = \frac{g}{\rho_c f} \frac{\partial \rho}{\partial y} \tag{3}$$

where ρ_c is the reference density of seawater and f is the Coriolis parameter. The eastward thermal wind surface velocities are calculated by integrating the meridional density gradient from the bottom to the surface of the ocean assuming the bottom velocities are zero. This neglects bottom-intensified currents, such as the deep western boundary currents, but yields very realistic surface velocities in the interior, as seen hereafter.

The role of wind forcing is also assessed. We examine both local forcing in the subpolar gyre and remote forcing

in the Southern Ocean. The former is gauged using the wind stress curl:

$$\vec{k} \cdot (\nabla \times \vec{\tau}) = \frac{1}{r_e \cos \theta} \left(\frac{\partial}{\partial \varphi} \tau^y - \frac{\partial}{\partial \theta} (\tau^x \cos \theta) \right) \tag{4}$$

where r_e is the radius of the Earth, θ and φ are latitude and longitude respectively, and τ^x and τ^y are the zonal and meridional components of the surface wind stress. The curl is related to the wind-driven circulation via the Sverdrup relation (Gill 1982). The changes in the curl are averaged over the subpolar gyre.

The wind forcing in the Southern Ocean is assessed via the zonally-integrated eastward wind stress, which is directly linked to the surface Ekman flux (Toggweiler and Samuels 1998; LaCasce and Isachsen 2010):

$$M_e = \frac{1}{\rho_c f(\theta)} \int_{-\delta}^0 \int_0^{360} \tau^x r_e \cos(\theta) d\phi dz \tag{5}$$

where δ is the depth of the Ekman layer and ϕ is the longitude. We integrate the winds at $\theta = 55^\circ\text{S}$, a latitude unblocked by continental boundaries.

3 Results

3.1 Overturning circulation changes in CMIP6

The 50-year mean global overturning streamfunction from the pre-industrial control run in the Norwegian Earth System Model, version 2.0 (NorESM2-LM, Seland et al. 2020; “NorESM2” hereafter) is shown in Fig. 1a. The shallower cell, in the upper 1000 m, has a maximum transport of 28 Sv (Sv = 10⁶ m³/s) and extends from the surface to just below 2000 m. The largest portion of this is in the Atlantic, the AMOC, with a maximum transport of 24 Sv. The deeper Antarctic Bottom Water (AABW) cell is also seen, as is the surface-intensified “Deacon Cell” between 40 and 60°S.

The corresponding 50-year mean overturning 100 years after the CO₂ quadrupling is shown in panel (b). The MOC has weakened greatly, to about 8.9 Sv, and is shallower. The AABW has also weakened substantially, indicating there is no bipolar seesaw compensation (Broecker 1999). On the other hand the Deacon Cell has actually strengthened somewhat, as discussed below.

The difference between the two overturning streamfunctions is shown in Fig. 1c. The AABW cell is nearly 10 Sv weaker, but the shallower cell declines even more, by nearly 20 Sv. The maximum difference is centered near 40°N and at a depth of around 1000 m. The location of maximum weakening and the shallowing of the shallow cell are consistent among the models. The observed change is dominated by the decline in AMOC.

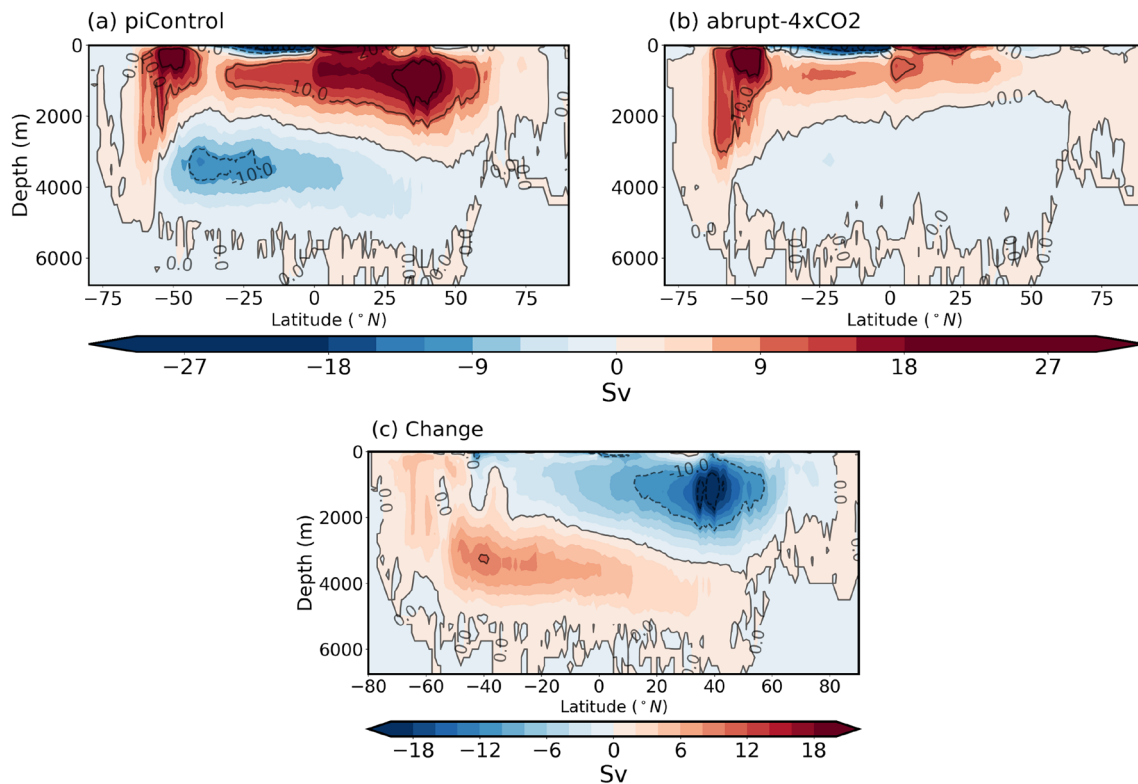


Fig. 1 The 50-year mean global meridional overturning mass streamfunction (Sv) for **a** the control run and **b** the 4xCO₂ run after 100 years in NorESM2. **c** shows the difference between the two. The red (blue) colour shows a clockwise (anti-clockwise) circulation

To compare the change in AMOC among the models, we calculate the maximum decrease between 20–50°N and 450–3000 m depth. The cell decreases in all models, but to differing degrees. The decline ranges from 5 to 22 Sv (Table 1), corresponding to a 15% to fully an 80% weakening (Fig. 2b). The GISS-E2-1-G simulation exhibits the largest reduction in overturning while the INM-CM4-8 run the least. The NorESM2 run (the orange dot) lies between these, with about a 60% decrease.

The temporal variation also varies between models (Fig. 2a). While AMOC reaches its minimum after only 20 years in some models, it takes 80 years in others. The AMOC in NorESM2 (orange curve) reaches its minimum around 40 years, recovers slightly and then settles thereafter. Given this, we use the period from 100 to 150 years to calculate averages for the perturbed model state.

3.2 Correlation with changes in wind stress

In most models, the winds change following the increase in CO₂. But the changes are inconsistent, increasing in some cases and decreasing in others.

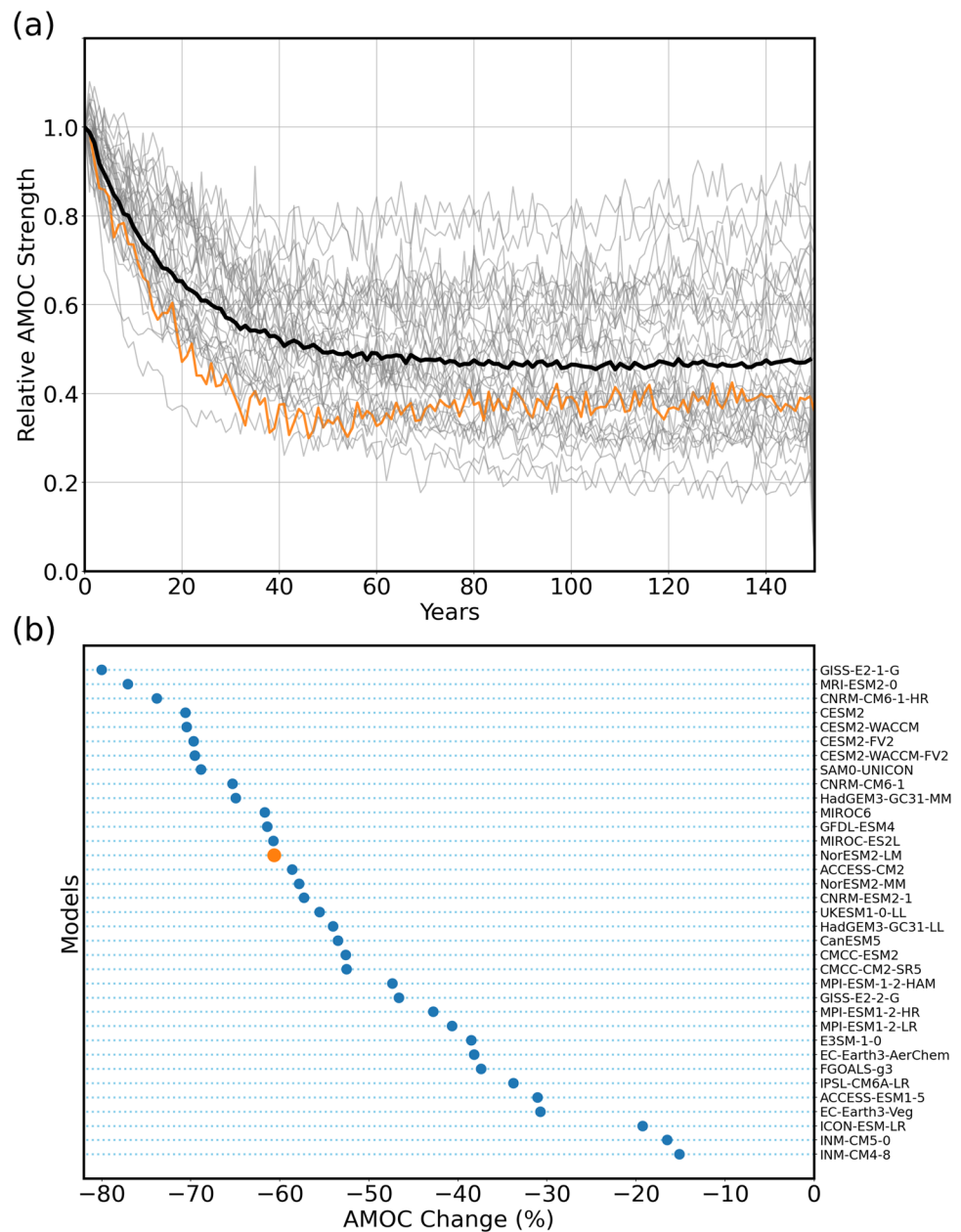
Consider the response in NorESM2. The wind stress curl in the control run is positive over the subpolar gyre and negative over the subtropical gyre (the solid and

dashed contours in Fig. 3a). Following the increase in CO₂, the curl weakens south of Greenland and over the Irminger and Labrador Seas, but strengthens south of the Gulf Stream (color contours in Fig. 3a). The other models behave similarly. All models exhibit weakening in the subpolar gyre, but the extent varies greatly.

To see whether the changes are correlated with those of AMOC, we averaged the difference in the curl over the subpolar gyre, i.e., 60°W–30°W, 50°N–60°N in all models. We then plotted the change in AMOC against the relative difference in curl (Fig. 3b) and calculated the Pearson correlation coefficient. The two measures are uncorrelated, with a correlation coefficient not significantly different from zero (based on the T test).

As noted, AMOC has also been linked to wind-driven Ekman transport in the Southern Ocean, following (Toggweiler and Samuels 1998). Thus, we also compared changes in the wind stress in the Southern Ocean with those in AMOC. The change in the zonal wind stress in the Southern Ocean in NorESM2 is shown in Fig. 4a. The winds have significantly strengthened in the circumpolar belt, and particularly in the South Pacific south of Australia (see also Chen et al. 2019). This results in a substantial increase in the northward Ekman transport (roughly 17 Sv in NorESM2).

Fig. 2 **a** Time series of annual-mean maximum Atlantic Meridional Overturning Circulation strength (AMOC) in 4xCO₂ simulation relative to its initial value in CMIP6. The thick black curve shows the multi-model mean. The mean percentage change in maximum AMOC strength in 4xCO₂ experiment relative to control run for the period 100–150 years for CMIP6 models is shown in **(b)**. NorESM2 is highlighted in orange in both plots



We averaged the change in the zonal wind stress, integrated zonally at 55°S, from all models and compared the result to the change in AMOC (Fig. 4b). In most models the integrated stress increases. The correlation with the change in AMOC however is weak and negative ($r = -0.28$, $p = 0.14$).

Thus, the change in Ekman transport in the Southern Ocean is unrelated to the decrease in AMOC in these simulations. The former instead causes an increase in the Deacon Cell, as seen in Fig. 1c. Indeed, that the Deacon Cell strengthens as AMOC weakens indicates the two are dynamically distinct over the adjustment period.

3.3 Correlation with changes in surface buoyancy

The surface density also changes in response to the forcing, and in a consistent way among the models. The change in the 50-year mean surface density from NorESM2 is shown in the left panel of Fig. 5. The surface density decreases dramatically north of the separated Gulf Stream (which we refer to as the NAC hereafter, for brevity) (Fig. 5). The greatest decreases are in the Labrador Sea, near Fram Strait and along a path extending from the east coast of North America to the tip of Greenland. The changes in

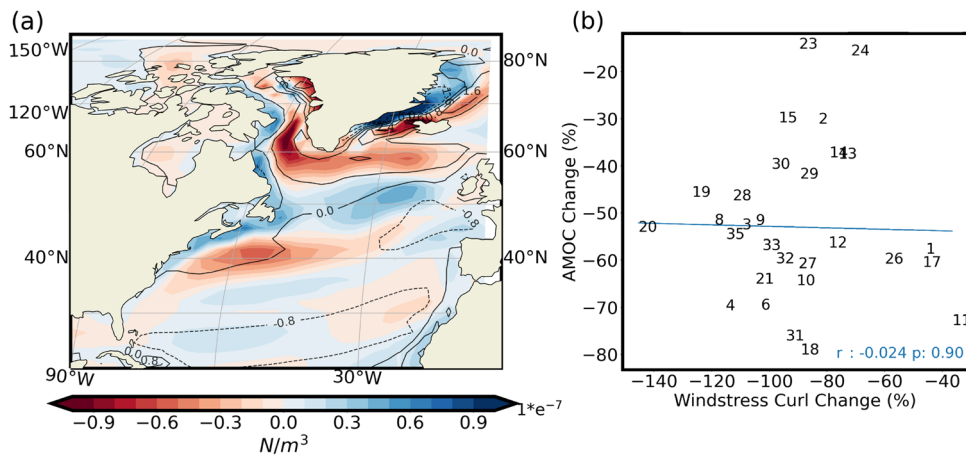


Fig. 3 a Spatial change in wind stress curl in 4xCO₂ simulation in NorESM2. Contours are superimposed to show the mean pre-industrial windstress curl. Mean change in wind stress curl in the sub-polar gyre in 4xCO₂ experiment relative to control for the period

100–150 years for CMIP6 models is shown in (b). Contours show $0.8 \times 10^{-7} \text{ N/m}^3$ intervals. The Pearson correlation coefficient (r) is shown in blue, with the significance level (p) from the T test. The numbers indicate CMIP6 models as listed in Table 1

Fig. 4 a Spatial change in zonal wind stress in the Southern Ocean in 4xCO₂ simulation in NorESM2. Mean change in the zonal wind stress in the Southern Ocean along Antarctic Circumpolar Current (ACC) in 4xCO₂ experiment relative to control for the period 100–150 years for CMIP6 models is shown in (b). Contours show $3 \times 10^{-2} \text{ N/m}^2$ intervals. The Pearson correlation coefficient (r) is shown in blue, with the significance level (p) from the T test. The numbers indicate CMIP6 models as listed in Table 1

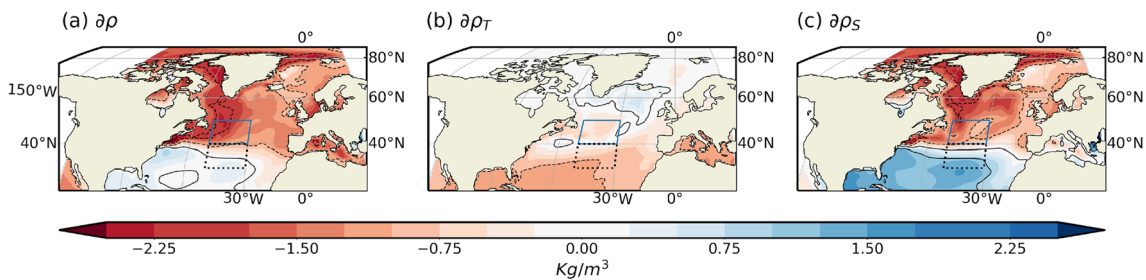
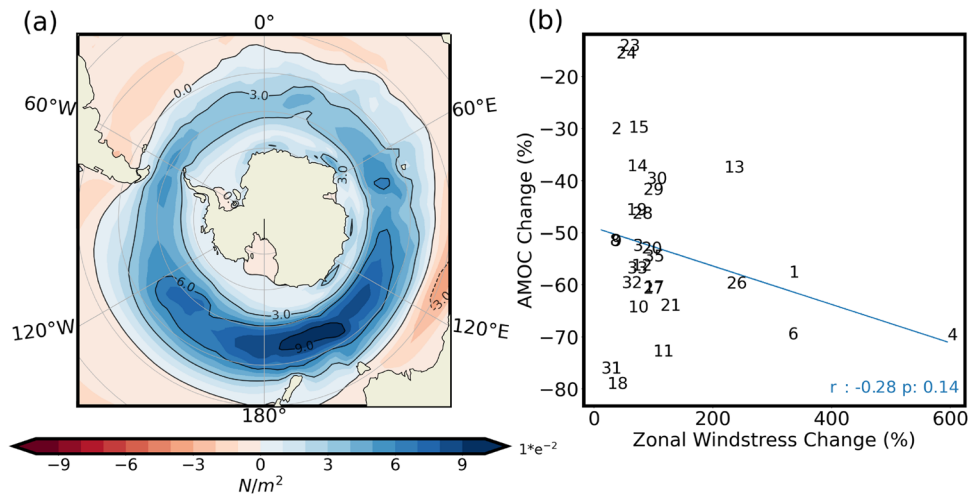


Fig. 5 Change in mean a surface density in 4xCO₂ experiment for NorESM2 relative to control simulation, due to b surface temperature and c surface salinity for the period 100–150 years. Contours show

1 Kg/m^3 intervals. The box denotes the area to the north (solid blue) and south (dotted black) of NAC where the density difference is calculated in Sect. 3.3

the subtropical North Atlantic are weaker, with a slight increase over much of the region.

The changes in the subpolar gyre are due largely to salinity (Fig. 5c). The surface waters are fresher in the western subpolar gyre, extending south from Greenland and along the path of the North Atlantic Current. They are also fresher in the Labrador Sea and in the northern Nordic Seas. The salinity-induced change in the subtropical gyre on the other hand is positive, due to increased evaporation.

At the same time, the subtropical gyre is warming (Fig. 5b). The resulting decrease in density nearly balances the increase due to evaporation, yielding relatively small changes in total density (see also Levang and Schmitt 2020b). In the northern subpolar gyre, there is cooling south of Greenland and Iceland. This is the so-called “cold blob” or “warming hole” (Drijfhout et al. 2012; Rahmstorf et al. 2015; Liu et al. 2020; Li et al. 2022; Ma et al. 2020). But the resulting increase in density is overwhelmed by the freshwater fluxes (Fig. 5c) so that the overall density change is negative.

Similar changes are seen in the other models. To test the relation with AMOC, we calculated the density difference between the subpolar and subtropical gyres, in the regions (50°W–40°W, 40°N–50°N) and (50°W–40°W, 30°N–40°N) (Fig. 5). This roughly captures the meridional density gradient across the NAC. We decomposed the density differences into temperature and density contributions and calculated the mean values in the perturbed experiment during the period 100–150 years. Those values were then differenced with the corresponding values from the control run and compared to the decrease in AMOC between the runs during the same period.

AMOC weakening is correlated with the change in surface density, with a correlation coefficient of $r = 0.531$ ($p = 0.004$) (Fig. 6a). Models which exhibit the largest decrease in the meridional density gradient exhibit the greatest weakening. The salinity-induced density change is

similarly correlated ($r = 0.525$, $p = 0.004$) (Fig. 6c). The temperature-induced change on the other hand is insignificantly anti-correlated with AMOC change ($r = -0.125$, $p = 0.52$). The correlations are negatively affected by a few outliers, in particular the models of NASA-GISS and MRI. Removing these two increases the correlation with both the surface density change ($r = 0.75$, $p = 0.00005$) and the salinity-induced change ($r = 0.733$, $p = 0.0001$) while leaving the relation to the temperature-induced gradient essentially unchanged.

The sequence of density changes in the North Atlantic from NorESM2 are shown in 5 year time averages in the Fig. 7a. Of particular interest is the tongue of light water which extends from Atlantic Canada into the interior, just north of the NAC. This is apparent even in the first 5 years, and intensifies thereafter.

Simultaneously, the velocities in the NAC weaken (Fig. 7b). During the first 5 years, the velocity decreases south of the NAC and strengthens to the north. Subsequently the weakening in the core of the NAC becomes evident. During the years 6–10, the decrease in velocities stretches back to the Florida Straits. The weakening intensifies after this, suggesting a near collapse of the NAC. Note too that the cyclonic flow in the eastern subpolar gyre and the southward flow east of Greenland both intensify.

The AMOC changes mirror those in the surface velocities (Fig. 7c). There is a weak adjustment during the first 5 years, except at the surface near the equator. The cell begins weakens dramatically subsequently, from years 5–10 and centered at 40°N. From years 10–20, the weakening intensifies and spreads with latitude, connecting to the weakened cell in the equatorial band.

The three fields are related. The tongue of freshwater which extends into the interior decreases the meridional density gradient across the NAC. This implies a weakening of its zonal velocity shear, $\partial u/\partial z$, from the thermal

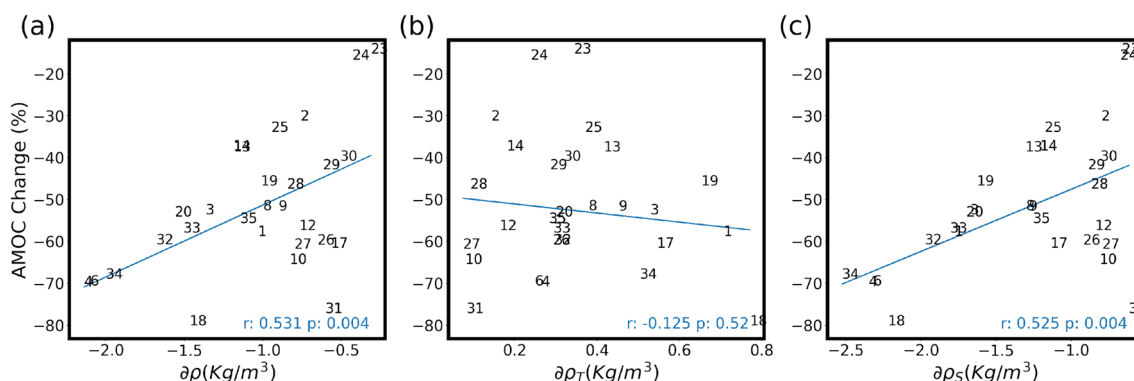


Fig. 6 Change in maximum AMOC strength for the period 100–150 years in the 4xCO₂ experiment relative to the control simulation plotted against **a** the change in the surface density difference across the NAC, **b** the corresponding density change due to temperature and

c the density change due salinity. The Pearson correlation coefficients (r) and significance levels (p) from the T test are inserted at the bottom right. As in Fig. 3, the numbers indicate CMIP6 models as listed in Table 1

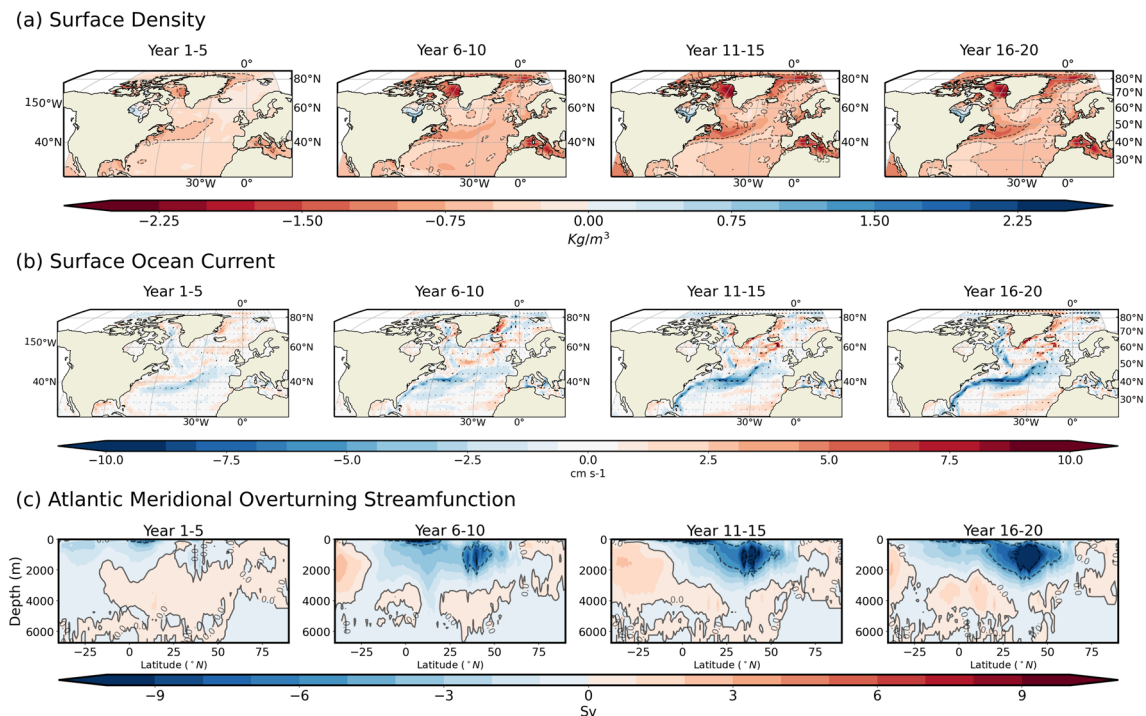


Fig. 7 Changes in surface density (Kg/m^3) (a), ocean currents (cm/s) at the surface (b), and Atlantic meridional overturning streamfunction (Sv) (c). Contours show 1 Kg/m^3 and 10 Sv intervals in (a) and (c) k, respectively. The change is calculated by subtracting the control

experiment 50-year means for each of the variable from the respective five-year means from the $4\times\text{CO}_2$ experiment. Year 1 is the year when CO_2 is abruptly quadrupled

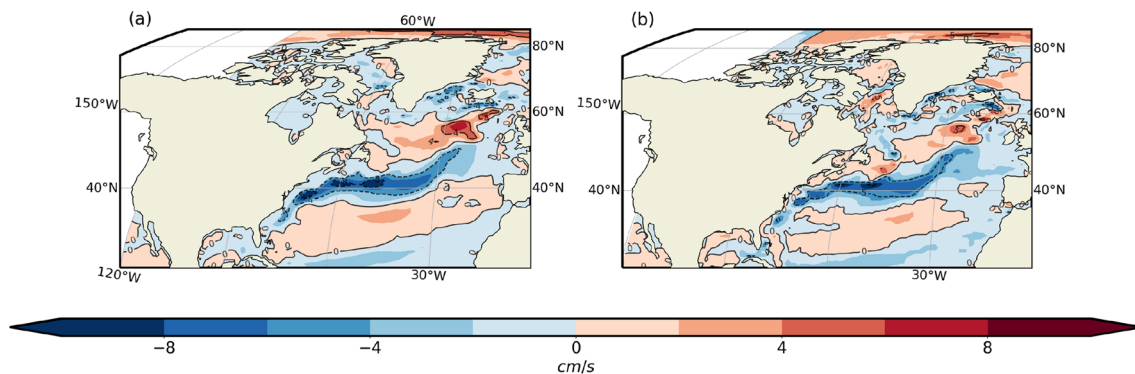


Fig. 8 Change in the mean zonal velocities from the vertically-integrated thermal wind (a). The change in the surface currents from the model are shown in (b) for comparison. Both fields are from

NorESM2 from the period 16–20 years after the quadrupling of CO_2 . Contours show 4 cm/s intervals

wind relation (Eq. 3) and hence a decrease in the surface velocities. To illustrate this, we integrate the thermal wind relation from the ocean bottom, assuming no flow there, and compare the resulting zonal velocity differences with those obtained in the model. The two fields, from the period 16–20 years, are nearly identical (Fig. 8). Thus the reduction in the meridional density gradient across the NAC directly reduces its transport.

Initially the freshwater tongue weakens the density gradient on its southern side but strengthens the gradient to the north. This is the reason for the dipolar response during the first 5 years, with the speeds increasing north of the separated Gulf Stream and decreasing to the south (Year 1–5 of Fig. 7b). As the lighter water spreads into the subpolar gyre, the dominant effect is the weakened gradient to the south, decreasing the NAC transport.

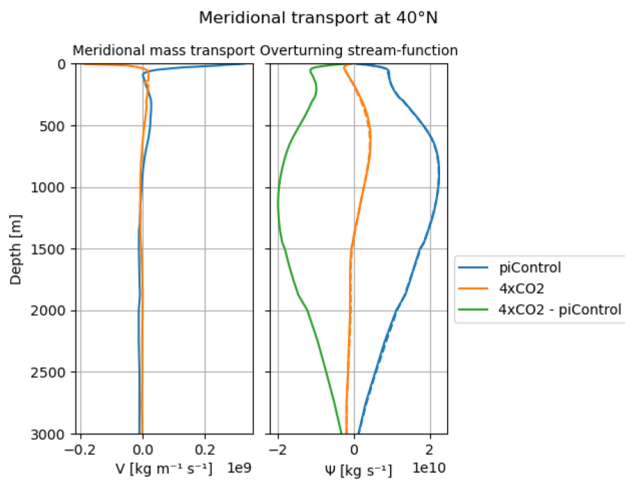


Fig. 9 The zonally-integrated meridional transport at 40°N as a function of depth (left panel) in NorESM2, and the corresponding overturning streamfunction (right panel). The transports have been converted to Kg/s, using the ocean density. The streamfunction curves are cumulative sums of the left curves, integrating downward from the surface. These are compared to the model’s own streamfunction curves, plotted as the dashed curves in the right panel

The weakened zonal transport implies a decreased meridional flow towards the subpolar gyre, and this directly impacts the AMOC cell. This is reflected in the overturning streamfunction at 40°N (Fig. 9), obtained by integrating the meridional velocity zonally and vertically, as in equation 3. The meridional mass transport changes most dramatically at the surface, even reversing sign in the 4xCO2 run. But the subsurface transport weakens as well, both northward at 500 m depth and southward below 1000 m.

As the velocities are integrated downward, the changes in the upper 500 m are mirrored deeper down. Note the

overturning streamfunction goes to zero at depth, so that the southward flow, which is primarily in a deep western boundary current, is weakening simultaneously. This is due to incompressibility; if only the inflow were decreasing, there would be a mass deficit at high latitudes.

Thus as the density gradient decreases at 40°N, the NAC transport declines, and the AMOC streamfunction mirrors this. As the velocity deficit spreads to the Florida Current, which is shallower, the AMOC weakening spreads southwards. And as the inflow to the subpolar gyre weakens, AMOC changes there as well.

3.4 Freshwater sources

The central element in AMOC weakening in these simulations is then the spreading of freshwater from the western boundary. The freshwater fluxes come from land runoff, precipitation and melting sea ice.

Time series of the fluxes north of 60°N in NorESM2 during the 150 years after the increase in CO₂ are plotted in Fig. 10a. Initially, the largest components are from sea ice (in orange) and runoff (dotted blue), while the contribution from precipitation minus evaporation (dotted green) is less than a third as large. During the first 10–20 years, the sea ice flux declines precipitously, to approximately the same level as P–E. This is due to the widespread loss of sea ice under the warming, primarily in the Arctic. In contrast, the runoff increases somewhat and then levels off, and P–E is nearly constant. The net effect is that the total freshwater flux decreases during the first 20 years and fluctuates around a constant value thereafter.

The decrease in freshwater fluxes occurs simultaneously with the decline in AMOC (Fig. 10b). The flux (smoothed with a 5 year moving filter) decreases during the first

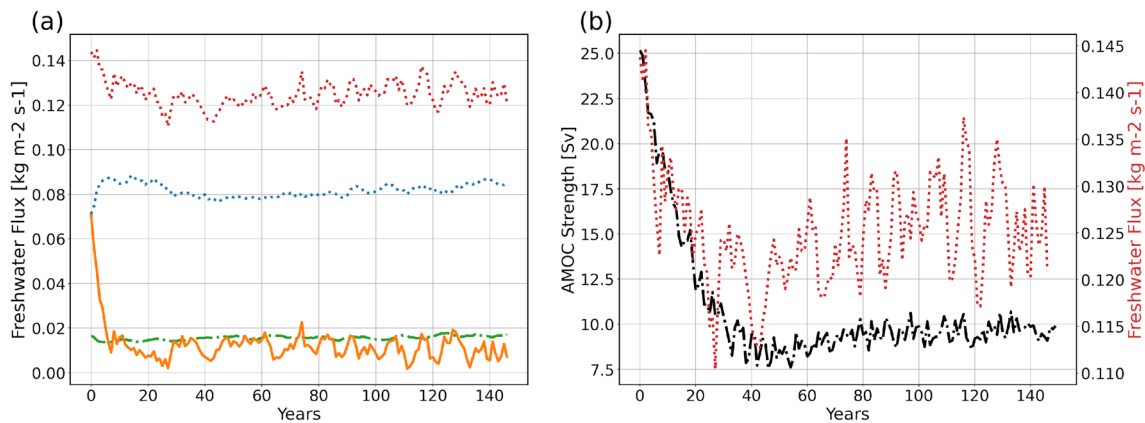


Fig. 10 a Freshwater flux components for the 150 years after increasing CO₂, from runoff (dotted blue), sea ice (orange) and precipitation minus evaporation (green dash-dot). The sum is shown by the dotted red curve. **b** The total freshwater flux (red dots) plotted with the

decrease in AMOC (black dash-dot). The freshwater fluxes have been smoothed with a 5 year running average for clarity. The first 2 years show annual values

20 years, as does AMOC. When the fluxes reach their new equilibrium thereafter, the AMOC curve flattens out. Thus the large release of freshwater primarily from sea ice melting and coincides with the AMOC weakening.

The 20 year adjustment period in part reflects the time required for freshwater to exit the Nordic and Labrador Seas and enter the subpolar gyre. This occurs in stages, as shown in Fig. 11. Even at year 2 (panel a), anomalous freshening is seen in the subpolar gyre. This can be traced to freshwater from the Gulf of St. Lawrence and, to a lesser extent, the Labrador Sea. By year 4, the northern Labrador Sea and the region east of Greenland are significantly fresher, and the signal is established north of the NAC by year 6. The connection with the Labrador Sea is clear by year 10, intensified along the western boundary. The connection with the Nordic Seas is evident later, after year 12. All sources feed the western boundary current and enter the interior north of the NAC.

The evolution is similar in the other models, although the exact route taken by the freshwater varies. In some cases, freshwater surges directly south from the Nordic Seas, flushing the northern subpolar gyre. But more typically the water moves in the western boundary current.

The diversity of weakened AMOC states seen in Fig. 2 reflects differing amounts of sea ice melt. In models with substantial Arctic sea ice melt, the AMOC is weakened the most. Increased meltwater production freshens the subpolar gyre to a greater extent, weakening the density contrast

across the Gulf Stream and hence the meridional flow of the NAC.

4 Discussion

The models in the CMIP6 ensemble exhibit consistent weakening of AMOC when CO_2 is abruptly quadrupled, with a multi-model average of 52%. The increase in CO_2 triggers extensive Arctic warming, which induces widespread melting of sea ice. This results in a large freshwater fluxes to the ocean during the first decade. The freshwater flows south along the eastern coast of North America and then eastward, north of the Gulf Stream. This decreases the density of the near-surface waters in the subpolar gyre. At the same time, the density changes little in the subtropical gyre, as surface warming is largely balanced by increased evaporation. Thus the density gradient across the North Atlantic Current is decreased, due to the fresher subpolar gyre. This weakens the vertical shear in the NAC and consequently its transport.

The CMIP6 models vary greatly in the extent of AMOC weakening, from 15 to 80%. This spread reflects the different freshwater production in the models. As the summer sea ice extent is reduced to zero in nearly all the models, the difference likely reflects the range of ice present initially. The exact route the freshwater takes when entering the subpolar gyre is also important. This causes deviations in the timing of AMOC weakening, from roughly 20 to 80 years (Fig. 2a).

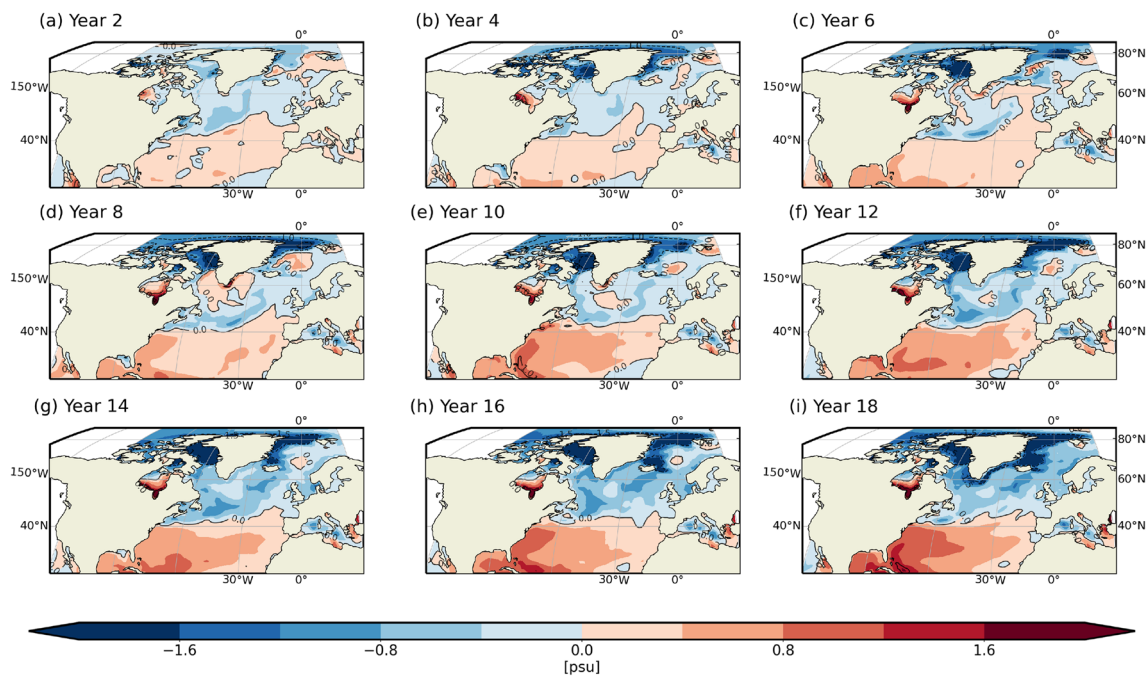


Fig. 11 Change in sea surface salinity in NorESM2 for the first 20 years after CO_2 is quadrupled for NorESM2-LM. The change is calculated by subtracting the control experiment 50-year mean from the respective annual means from 4x CO_2 experiment

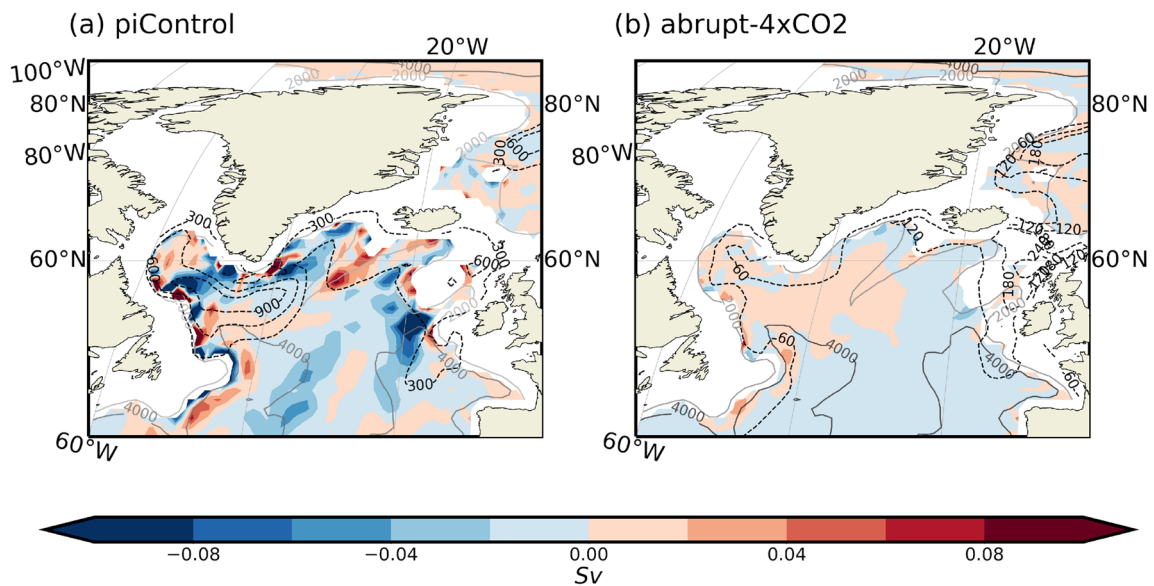


Fig. 12 50-year-mean vertical ocean mass transport at 1000 m in piControl (a) and 4xCO₂ (b) 100 years after the quadrupling of CO₂ from NorESM2. Dotted black contours show mean of the maximum ocean mixed layer depth define by sigma T for the same period

for the two experiments. The contour interval is 300 m in (a), but it is reduced to 60 m in (b) for clarity. Gray contours show 2000 m isobaths the model bathymetry

Changes in local (subpolar) and remote winds were uncorrelated with AMOC weakening in these models. That is not to say wind forcing is unimportant; sub-decadal variability, which is pronounced, owes much to wind forcing. But the response to the drastic forcing in this scenario is buoyancy-driven in these simulations.

Dai (2022) noted the connection between Arctic amplification and a weakening AMOC, in simulations in which CO₂ was increased by 1% per year. That study linked the decrease in overturning to the meridional density gradient, as argued here, but also to reduced mixed layer depths, as claimed in other studies. In contrast, de Boer et al. (2010) contended that AMOC strength and the meridional density gradient were poorly correlated; the gradient in their case was between the equator and North Atlantic however, rather than across the NAC. The authors also found a positive correlation with the wind stress in the Southern Ocean, which was absent in the present simulations. Levang and Schmitt (2020a) concluded that salinity was less important for AMOC weakening in CMIP5 simulations than temperature. Their focus was on the zonal density gradient, at depths greater than 1000 m. They noted too that the increase in density due to evaporation was offset by warming. But as seen here, that applies to the subtropical gyre; changes in the subpolar gyre are dominated by salinity, and this is what correlates with the weakened NAC in CMIP6. And Bonan et al. (2022) concluded that subsurface temperature changes in the deep water formation regions were responsible for AMOC weakening, in millennial length simulations under

quadrupled CO₂. Salinity changes in the same regions preceded AMOC recovery in some models. We did not examine whether such changes occur in the present simulations.

The present study supports the relevance of “hosing experiments”, in which freshwater is introduced at high latitudes (Mecking et al. 2016; Jackson et al. 2016; Haskins et al. 2018; Jackson et al. 2022). In these, freshwater is usually added uniformly, typically over the entire subpolar gyre. In the North Atlantic hosing model intercomparison project (NAHosMIP), 0.3 Sv of freshwater was added uniformly north of 50°N for 50–100 years, and this led to AMOC weakening in all the models. The present simulations differ because the freshwater in most cases follows the western boundary before entering the subpolar gyre north of the Gulf Stream separation. If applied uniformly, the impact on the meridional density gradient could differ. A more realistic approach might be to apply hosing solely in the Labrador Sea, for example.

The connection between freshwater production at high latitudes and AMOC weakening has been made before (see Weijer et al. 2022 and references therein). But the reason usually given is that freshwater “caps the convective regions”, preventing deep water formation. We posit instead that freshwater *weakens the inflow* to the high latitude regions, by altering the meridional density gradient. This view is consistent with the study of Gjermundsen et al. (2018), in which the AMOC and AABW cells were successively weakened in an ocean GCM simply by altering the surface density gradient. Consistently, the extent of AMOC

weakening in the CMIP6 models depends on the volume of freshwater introduced to the subpolar gyre, which explains the large spread of AMOC weakening among the models. Such a connection has not been made previously with respect to the convective hypothesis; indeed, it is unclear how different degrees of “capping” could reduce AMOC by different amounts.

The focus on the convective regions began, arguably, with the idealized models of Stommel and Arons (1959), which examined the abyssal circulation resulting from specified deep water sources in different locations. In more realistic settings, dense water is formed in boundary currents rather than in the centers of the gyres in the Labrador, Greenland and Norwegian Seas, where convection is typically observed (Mauritzen 1996; Spall and Pickart 2001). This is the case in the present simulations as well. The mixed layer depths in the Labrador and Irminger Seas decrease as AMOC weakens (Fig. 12), due primarily to warmer air temperatures. But here too the sinking occurs primarily along the boundaries (left panel), adjacent to the regions with the deepest mixed layers. Indeed, the mixed layer depths also decrease in the Nordic Seas, but the exchange across the Greenland-Scotland ridge is very modest in these models, implying the convection in the Nordic Seas is local and seasonal. Downwelling thus appears to be part of the larger scale circulation stemming from the surface meridional density gradient, as suggested by Gjermundsen and LaCasce (2017), Gjermundsen et al. (2018).

How long does the weakened state persist? In the present 4xCO₂ simulations, AMOC remains weak in all models for at least 150 years. In contrast, in half the simulations in the NAHosMIP study, AMOC recovered after the freshwater hosing ceased (Jackson et al. 2022). Following the present arguments, the weakened state should persist as long as the meridional density gradient remains weak. If the excess freshwater in the subpolar gyre were exported, the gradient could presumably strengthen again (Liu et al. 2014). This could trigger AMOC recovery, like that described by Bonan et al. (2022). The NAC is a barrier to mixing, hindering such export, but this presumably occurs over longer time scales. We are currently examining this, using longer simulations.

There are numerous caveats about the CMIP6 models. Dense water formation occurs primarily south of Greenland, rather than in the Nordic Seas, for one. The models also employ a range of different sea ice models, which will impact the freshwater input to the ocean. Nevertheless, the link between AMOC and the meridional density gradient across the NAC is dynamically plausible and consistent with previous studies with more idealized ocean models. The results also suggest a straightforward way to model future changes in AMOC, by monitoring salinity north of the NAC.

Appendix: List of CMIP6 models used

See Table 1.

Table 1 List of CMIP6 models used for the analyses of ocean and atmosphere variables

No	Model	$\Psi_{control}$ (Sv)	Ψ_{4xCO_2} (Sv)	Ψ_{Change} (%)	Variant label	Reference
1	ACCESS-CM2	21.88	9.05	- 12.83 (- 58.6)	rli1p1f1	Bi et al. (2020)
2	ACCESS-ESM1-5	23.45	16.16	- 7.29 (- 31.1)	rli1p1f1	Ziehn et al. (2020)
3	CanESM5	14.96	6.96	- 8 (- 53.5)	rli1p2f1	Swart et al. (2019)
4	CESM2	24.52	7.2	- 17.32 (- 70.6)	rli1p1f1	Danabasoglu et al. (2020)
5	CESM2-FV2	25.15	7.62	- 17.53 (- 69.7)	rli1p1f1	Danabasoglu et al. (2020)
6	CESM2-WACCM	24.47	7.22	- 17.25 (- 70.5)	rli1p1f1	Danabasoglu et al. (2020)
7	CESM2-WACCM-FV2	25.97	7.9	- 18.07 (- 69.6)	rli1p1f1	Danabasoglu et al. (2020)
8	CMCC-CM2-SR5	24.55	11.66	- 12.89 (- 52.5)	rli1p1f1	Cherchi et al. (2018)
9	CMCC-ESM2	23.24	11.02	- 12.22 (- 52.6)	rli1p1f1	Lovato et al. (2022)
10	CNRM-CM6-1	23.7	8.21	- 15.49 (- 65.4)	rli1p1f2	Voldoire et al. (2019)
11	CNRM-CM6-1-HR	18.37	4.81	- 13.56 (- 73.8)	rli1p1f2	Voldoire et al. (2019)
12	CNRM-ESM2-1	20.82	8.89	- 11.93 (- 57.3)	rli1p1f2	Séférian et al. (2019)
13	E3SM-1-0	18.16	11.17	- 6.99 (- 38.5)	rli1p1f1	Golaz et al. (2019)
14	EC-Earth3-AerChem	19.63	12.14	- 7.49 (- 38.2)	rli1p1f1	Döscher et al. (2022)
15	EC-Earth3-Veg	18.71	12.96	- 5.75 (- 30.7)	rli1p1f1	Döscher et al. (2022)
16	FGOALS-g3	40	25.05	- 14.95 (- 37.4)	rli1p1f1	He et al. (2019)
17	GFDL-ESM4	23.81	9.19	- 14.62 (- 61.4)	rli1p1f1	Dunne et al. (2020)
18	GISS-E2-1-G	28.96	5.79	- 23.17 (- 80.0)	rli1p1f1	Schmidt et al. (2014)
19	GISS-E2-2-G	30.31	16.18	- 14.13 (- 46.6)	rli1p3f1	Rind et al. (2020)
20	HadGEM3-GC31-LL	18.66	8.58	- 10.08 (- 54.0)	rli1p1f1	Kuhlbrodt et al. (2018)
21	HadGEM3-GC31-MM	20.48	7.17	- 13.31 (- 65.0)	rli1p1f1	Williams et al. (2018)
22	ICON-ESM-LR	22.49	18.16	- 4.33 (- 19.3)	rli1p1f1	Jungclaus et al. (2022)
23	INM-CM4-8	21.88	18.57	- 3.31 (- 15.1)	rli1p1f1	Volodin et al. (2018)
24	INM-CM5-0	21.16	17.67	- 3.49 (- 16.5)	rli1p1f1	Volodin et al. (2017)
25	IPSL-CM6A-LR	14.12	9.35	- 4.77 (- 33.8)	rli1p1f1	Boucher et al. (2020)
26	MIROC-ES2L	16.86	6.61	- 10.25 (- 60.8)	rli1p1f2	Hajima et al. (2020)
27	MIROC6	20.18	7.73	- 12.45 (- 61.7)	rli1p1f1	Tatebe et al. (2019)
28	MPI-ESM-1-2-HAM	25.18	13.26	- 11.92 (- 47.3)	rli1p1f1	Tegen et al. (2019), Neubauer et al. (2019)
29	MPI-ESM1-2-HR	21.67	12.4	- 9.27 (- 42.8)	rli1p1f1	Müller et al. (2018)
30	MPI-ESM1-2-LR	24.23	14.37	- 9.86 (- 40.7)	rli1p1f1	Mauritsen et al. (2019)
31	MRI-ESM2-0	22.86	5.24	- 17.62 (- 77.1)	rli2p1f1	Yukimoto et al. (2019)
32	NorESM2-LM	24.42	9.61	- 14.81 (- 60.6)	rli1p1f1	Seland et al. (2020)
33	NorESM2-MM	24.69	10.4	- 14.29 (- 57.9)	rli1p1f1	Seland et al. (2020)
34	SAM0-UNICON	27.18	8.46	- 18.72 (- 68.9)	rli1p1f1	Park et al. (2019)
35	UKESM1-0-LL	17.91	7.97	- 9.94 (- 55.5)	rli1p1f2	Sellar et al. (2019)

For each model, 50-year-mean AMOC strength after 100 years for the control and 4xCO₂, change and relative change are calculated for the 35 models

Acknowledgements We are grateful to two anonymous reviewers for constructive suggestions on the original manuscript.

Author contributions JHL conceived the project and led the analysis. CI performed the initial calculations with NorESM2 data, as part of her masters thesis. GM expanded the analysis to include the full suite of CMIP6 models. AG contributed with diverse analyses on all aspects. All authors contributed to writing and editing the article.

Funding Open access funding provided by University of Oslo (incl Oslo University Hospital). GM was supported by a grant from the Department of Education in Norway. AG received support from the Norwegian Research Council funded projects INES (270061) and Key-Clim (295046). JHL was supported under the Rough Ocean project, number 302743, from the Norwegian Research Council.

Availability of data and materials The CMIP6 model data used is available from the Earth System Grid Federation (ESGF) server at <https://esgf-node.llnl.gov/search/cmip6/> last accessed in December, 2022.

Code availability All code used in the analysis is available on request.

Declarations

Conflict of interest The authors have no conflicts of interest.

Ethics approval Not applicable.

Consent to participate Not applicable.

Consent for publication Not applicable.

Open Access This article is licensed under a Creative Commons Attribution 4.0 International License, which permits use, sharing, adaptation, distribution and reproduction in any medium or format, as long as you give appropriate credit to the original author(s) and the source, provide a link to the Creative Commons licence, and indicate if changes were made. The images or other third party material in this article are included in the article's Creative Commons licence, unless indicated otherwise in a credit line to the material. If material is not included in the article's Creative Commons licence and your intended use is not permitted by statutory regulation or exceeds the permitted use, you will need to obtain permission directly from the copyright holder. To view a copy of this licence, visit <http://creativecommons.org/licenses/by/4.0/>.

References

- Bakker P (2016) Fate of the Atlantic meridional overturning circulation: strong decline under continued warming and Greenland melting. *Geophys Res Lett* 43:12–25212260. <https://doi.org/10.1002/2016GL070457>
- Bi D, Dix M, Marsland S, O'Farrell S, Sullivan A, Bodman R, Law R, Harman I, Srbinovsky J, Rashid HA, Dobrohotoff P, Mackallah C, Yan H, Hirst A, Savita A, Dias FB, Woodhouse M, Fiedler R, Heerdegen A (2020) Configuration and spin-up of ACCESS-CM2, the new generation Australian community climate and earth system simulator coupled model. *J South Hemisphere Earth Syst Sci* 70(1):225. <https://doi.org/10.1071/es19040>
- Bonan D, Thompson A, Newsom E, Sun S, Rugenstein M (2022) Transient and equilibrium responses of the Atlantic overturning circulation to warming in coupled climate models: the role of temperature and salinity. *J Clim* 35(15):5173–5193. <https://doi.org/10.1175/JCLI-D-21-0912.1>
- Boucher O, Servonnat J, Albright AL, Aumont O, Balkanski Y, Bastrikov V, Bekki S, Bonnet R, Bony S, Bopp L, Braconnot P, Brockmann P, Cadule P, Caubel A, Cheruy F, Codron F, Cozic A, Cugnet D, D'Andrea F, Davini P, de Lavergne C, Denvil S, Deshayes J, Devilliers M, Ducharne A, Dufresne J-L, Dupont E, Éthé C, Fairhead L, Falletti L, Flavoni S, Foujols M-A, Gardoll S, Gastineau G, Ghattas J, Grandpeix J-Y, Guenet B, Lionel EG, Guilyardi E, Guimberteau M, Hauglustaine D, Hourdin F, Idelkadi A, Joussaume S, Kageyama M, Khodri M, Krinner G, Lebas N, Levassasseur G, Lévy C, Li L, Lott F, Lurton T, Luysaert S, Madec G, Madeleine J-B, Maignan F, Marchand M, Marti O, Mellul L, Meurdesoif Y, Mignot J, Musat I, Ottlé C, Peylin P, Planton Y, Polcher J, Rio C, Rochetin N, Rousset C, Sepulchre P, Sima A, Swingedouw D, Thiéblemont R, Traore AK, Vancoppenolle M, Vial J, Vialard J, Viovy N, Vuichard N (2020) Presentation and evaluation of the IPSL-CM6a-LR climate model. *J Adv Model Earth Syst.* <https://doi.org/10.1029/2019ms002010>
- Bower A, Lozier S, Biastoch A, Drouin K, Foukal N, Furey H, Lankhorst M, Rühls S, Zou S (2019) Lagrangian views of the pathways of the Atlantic meridional overturning circulation. *J Geophys Res Oceans* 124(8):5313–5335. <https://doi.org/10.1029/2019JC015014>
- Broecker W (1991) The great ocean conveyor. *Oceanography* (Washington, DC.) 4(2):79–89. <https://doi.org/10.5670/oceanog.1991.07>
- Broecker WS (1999) Paleocirculation during the last deglaciation: a bipolar seesaw? *Paleoceanography* 13:119–121. <https://doi.org/10.1029/97PA03707>
- Bryden HL, Longworth HR, Cunningham SA (2005) Slowing of the Atlantic meridional overturning circulation at 25 degrees N. *Nature* 438(7068):655–657. <https://doi.org/10.1038/nature04385>
- Bryden HL, Longworth HR, Cunningham SA (2005) Slowing of the Atlantic meridional overturning circulation at 25°N. *Nature* 438(7068):655–657. <https://doi.org/10.1038/nature04385>
- Caínzos V, Hernández-Guerra A, McCarthy GD, McDonagh EL, Armas MC, Pérez-Hernández MD (2022) Thirty years of GOSHIP and WOCE data: Atlantic overturning of mass, heat, and freshwater transport. *Geophys Res Lett.* <https://doi.org/10.1029/2021gl096527>
- Cessi P (2019) The global overturning circulation. *Annu Rev Mar Sci* 11(1):249–270. <https://doi.org/10.1146/annurev-marine-010318-095241>
- Chen C, Liu W, Wang G (2019) Understanding the uncertainty in the 21st century dynamic sea level projections: the role of the AMOC. *Geophys Res Lett* 46(1):210–217. <https://doi.org/10.1029/2018gl080676>
- Cheng W, Chiang JCH, Zhang D (2013) Atlantic meridional overturning circulation (AMOC) in CMIP5 models: RCP and historical simulations. *J Clim* 26(18):7187–7197. <https://doi.org/10.1175/JCLI-D-12-00496.1>
- Cherchi A, Fogli PG, Lovato T, Peano D, Iovino D, Gualdi S, Masina S, Scoccimarro E, Matera S, Bellucci A, Navarra A (2018) Global mean climate and main patterns of variability in the CMCC-CM2 coupled model. *J Adv Model Earth Syst.* <https://doi.org/10.1029/2018ms001369>
- Dai A (2022) Arctic amplification is the main cause of the Atlantic meridional overturning circulation weakening under large CO₂ increases. *Clim Dyn* 58:3243–3259. <https://doi.org/10.1007/s00382-021-06096-x>
- Danabasoglu G, Lamarque J-F, Bacmeister J, Bailey DA, DuVivier AK, Edwards J, Emmons LK, Fasullo J, Garcia R, Gettelman A, Hannay C, Holland MM, Large WG, Lauritzen PH, Lawrence DM, Lenaerts JTM, Lindsay K, Lipscomb WH, Mills MJ, Neale R, Oleson KW, Otto-Bliessen B, Phillips AS, Sacks W, Tilmes S, Kampenhou L, Verstein M, Bertini A, Dennis J, Deser C, Fischer C, Fox-Kemper B, Kay JE, Kinnison D, Kushner PJ, Larson VE, Long MC, Mickelson S, Moore JK, Nienhouse E, Polvani L, Rasch PJ, Strand WG (2020) The community Earth system model version 2 (CESM2). *J Adv Model Earth Syst.* <https://doi.org/10.1029/2019ms001916>
- de Boer AM, Gnanadesikan A, Edwards NR, Watson AJ (2010) Meridional density gradients do not control the Atlantic overturning circulation. *J Phys Oceanogr* 40:368–380. <https://doi.org/10.1175/2009JPO4200.1>
- de Verdière AC (1988) Buoyancy driven planetary flows. *J Mar Res* 46:215–265
- Delworth TL, Mann ME (2000) Observed and simulated multidecadal variability in the northern hemisphere. *Clim Dyn* 16(9):661–676. <https://doi.org/10.1007/s003820000075>
- Dixon KW, Delworth TL, Spelman MJ, Stouffer RJ (1999) The influence of transient surface fluxes on north Atlantic overturning in

- a coupled GCM climate change experiment. *Geophys Res Lett* 26(17):2749–2752. <https://doi.org/10.1029/1999gl900571>
- Döscher R, Acosta M, Alessandri A, Anthoni P, Arsouze T, Bergman T, Bernardello R, Boussetta S, Caron L-P, Carver G, Castrillo M, Catalano F, Cvijanovic I, Davini P, Dekker E, Doblas-Reyes FJ, Docquier D, Echevarria P, Fladrich U, Fuentes-Franco R, Gröger M, Hardenberg vJ, Hieronymus J, Karami MP, Keskinen J-P, Koenigk T, Makkonen R, Massonnet F, Ménégos M, Miller PA, Moreno-Chamarro E, Nieradzick L, van Noije T, Nolan P, O'Donnell D, Ollinaho P, van den Oord G, Ortega P, Prims OT, Ramos A, Reerink T, Rousset C, Ruprich-Robert Y, Sager PL, Schmith T, Schrödner R, Serva F, Sicardi V, Madsen MS, Smith B, Tian T, Tourigny E, Uotila P, Vancoppenolle M, Wang S, Wärlind D, Willén U, Wyser K, Yang S, Yepes-Arbós X, Zhang Q (2022) The EC-Earth3 Earth system model for the coupled model intercomparison project 6. *Geosci Model Dev* 15(7):2973–3020. <https://doi.org/10.5194/gmd-15-2973-2022>
- Drijfhout S, Hazeleger W (2007) Detecting Atlantic MOC changes in an ensemble of climate change simulations. *J Clim* 20:1571–1582. <https://doi.org/10.1175/JCLI4104.1>
- Drijfhout S, van Oldenborgh GJ, Cimadoribus A (2012) Is a decline of AMOC causing the warming hole above the north Atlantic in observed and modeled warming patterns? *J Clim* 25(24):8373–8379. <https://doi.org/10.1175/JCLI-D-12-00490.1>
- Dunne JP, Horowitz LW, Adcroft AJ, Ginoux P, Held IM, John JG, Krasting JP, Malyshev S, Naik V, Paulot F, Shevliakova E, Stock CA, Zadeh N, Balaji V, Blanton C, Dunne KA, Dupuis C, Durachta J, Dussin R, Gauthier PPG, Griffies SM, Guo H, Hallberg RW, Harrison M, He J, Hurlin W, McHugh C, Menzel R, Milly PCD, Nikonov S, Paynter DJ, Ploshay J, Radhakrishnan A, Rand K, Reichl BG, Robinson T, Schwarzkopf DM, Sentman LT, Underwood S, Vahlenkamp H, Winton M, Wittenberg AT, Wyman B, Zeng Y, Zhao M (2020) The GFDL earth system model version 4.1 (GFDL-ESM 4.1): overall coupled model description and simulation characteristics. *J Adv Model Earth Syst*. <https://doi.org/10.1029/2019ms002015>
- Eyring V, Bony S, Meehl GA, Senior CA, Stevens B, Stouffer RJ, Taylor KE (2016) Overview of the coupled model intercomparison project phase 6 (CMIP6) experimental design and organization. *Geosci Model Dev* 9(5):1937–1958. <https://doi.org/10.5194/gmd-9-1937-2016>
- Fofonoff NP, Millard RC (1983) Algorithms for the computation of fundamental properties of seawater. Technical report, UNESCO Technical Papers in Marine Science. <https://doi.org/10.25607/OBP-1450>
- Fox-Kemper B, Hewitt HT, Xiao C, Adalgeirsdottir G, Drijfhout SS, Edwards TL, Golledge NR, Hemer M, Kopp RE, Krinner G, Mix A, Notz D, Nowicki S, Nurhati IS, Ruiz L, Sallée J-B, Slangen ABA, Yu Y (2021) 2021: Ocean, cryosphere and sea level change. *Climate change 2021: the physical science basis. Contribution of Working Group I to the Sixth Assessment Report of the Intergovernmental Panel on Climate Change*, pp 1211–1362. <https://doi.org/10.1017/9781009157896.011>
- Fu Y, Li F, Karstensen J, Wang C (2020) A stable Atlantic meridional overturning circulation in a changing north Atlantic ocean since the 1990s. *Sci Adv* 6(48):7836. <https://doi.org/10.1126/sciadv.abc7836>
- Ganachaud A, Wunsch C (2003) Large-scale ocean heat and freshwater transports during the world ocean circulation experiment. *J Clim* 16(4):696–705. [https://doi.org/10.1175/1520-0442\(2003\)016<0696:LSOHAF>2.0.CO;2](https://doi.org/10.1175/1520-0442(2003)016<0696:LSOHAF>2.0.CO;2)
- Ganopolski A, Rahmstorf S (2001) Rapid changes of glacial climate simulated in a coupled climate model. *Nature* 409(6817):153–158. <https://doi.org/10.1038/35051500>
- Gill AE (1982) *Atmosphere-ocean dynamics* 30. Academic Press, London, pp 317–370. [https://doi.org/10.1016/S0074-6142\(08\)60034-0](https://doi.org/10.1016/S0074-6142(08)60034-0)
- Gjermundsen A, LaCasce JH (2017) Comparing the linear and nonlinear buoyancy-driven circulation. *Tellus* 69(1):1299282. <https://doi.org/10.1080/16000870.2017.1299282>
- Gjermundsen A, LaCasce JH, Denstad L (2018) The thermally driven ocean circulation with realistic bathymetry. *J Phys Oceanogr* 48(3):647–665. <https://doi.org/10.1175/JPO-D-17-0147.1>
- Golaz J-C, Caldwell PM, Roedel LPV, Petersen MR, Tang Q, Wolfe JD, Abeshu G, Anantharaj V, Asay-Davis XS, Bader DC, Baldwin SA, Bisht G, Bogenschütz PA, Branstetter M, Brunke MA, Brus SR, Burrows SM, Cameron-Smith PJ, Donahue AS, Deakin M, Easter RC, Evans KJ, Feng Y, Flanner M, Foucar JG, Fuke JG, Griffin BM, Hannay C, Harrop BE, Hoffman MJ, Hunke EC, Jacob RL, Jacobsen DW, Jeffery N, Jones PW, Keen ND, Klein SA, Larson VE, Leung LR, Li H-Y, Lin W, Lipscomb WH, Ma P-L, Mahajan S, Maltrud ME, Mamejanov A, McClean JL, McCoy RB, Neale RB, Price SF, Qian Y, Rasch PJ, Eyre JEJR, Riley WJ, Ringler TD, Roberts AF, Roesler EL, Salinger AG, Shaheen Z, Shi X, Singh B, Tang J, Taylor MA, Thornton PE, Turner AK, Veneziani M, Wan H, Wang H, Wang S, Williams DN, Wolfram PJ, Worley PH, Xie S, Yang Y, Yoon J-H, Zelinka MD, Zender CS, Zeng X, Zhang C, Zhang K, Zhang Y, Zheng X, Zhou T, Zhu Q (2019) The DOE e3sm coupled model version 1: overview and evaluation at standard resolution. *J Adv Model Earth Syst* 11(7):2089–2129. <https://doi.org/10.1029/2018ms001603>
- Gregory JM (2005) A model intercomparison of changes in the Atlantic thermohaline circulation in response to increasing atmospheric CO₂ concentration. *Geophys Res Lett* 32:12703. <https://doi.org/10.1029/2005GL023209>
- Gregory JM, Bouffes N, Griffies SM, Haak H, Hurlin WJ, Jungclaus J, Kelley M, Lee WG, Marshall J, Romanou A, Saenko OA, Stammer D, Winton M (2016) The flux-anomaly-forced model intercomparison project (FAFMIP) contribution to CMIP6: investigation of sea-level and ocean climate change in response to CO₂ forcing. *Geosci Model Dev* 9(11):3993–4017. <https://doi.org/10.5194/gmd-9-3993-2016>
- Hajima T, Watanabe M, Yamamoto A, Tatebe H, Noguchi MA, Abe M, Ohgaito R, Ito A, Yamazaki D, Okajima H, Ito A, Takata K, Ogochi K, Watanabe S, Kawamiya M (2020) Development of the MIROC-ES2l earth system model and the evaluation of biogeochemical processes and feedbacks. *Geosci Model Dev* 13(5):2197–2244. <https://doi.org/10.5194/gmd-13-2197-2020>
- Häkkinen S, Rhines PB (2004) Decline of subpolar north Atlantic circulation during the 1990s. *Science* 304(5670):555–559. <https://doi.org/10.1126/science.1094917>
- Haskins RK, Oliver KIC, Jackson LC, Drijfhout SS, Wood RA (2018) Explaining asymmetry between weakening and recovery of the AMOC in a coupled climate model. *Clim Dyn* 53(1–2):67–79. <https://doi.org/10.1007/s00382-018-4570-z>
- Haskins RK, Oliver KIC, Jackson LC, Wood RA, Drijfhout SS (2020) Temperature domination of AMOC weakening due to freshwater hosing in two GCMs. *Clim Dyn* 54(1–2):273–286. <https://doi.org/10.1007/s00382-019-04998-5>
- He F, Clark PU (2022) Freshwater forcing of the Atlantic meridional overturning circulation revisited. *Nat Clim Chang* 12(5):449–454. <https://doi.org/10.1038/s41558-022-01328-2>
- He B, Bao Q, Wang X, Zhou L, Wu X, Liu Y, Wu G, Chen K, He S, Hu W, Li J, Li J, Nian G, Wang L, Yang J, Zhang M, Zhang X (2019) CAS FGOALS-f3-l model datasets for CMIP6 historical atmospheric model intercomparison project simulation. *Adv Atmos Sci* 36(8):771–778. <https://doi.org/10.1007/s00376-019-9027-8>
- Hirschi J, Baehr J, Marotzke J, Stark J, Cunningham S, Beismann J-O (2003) A monitoring design for the Atlantic meridional

- overturning circulation. *Geophys Res Lett.* <https://doi.org/10.1029/2002GL016776>
- Hirschi J, Killworth P, Blundell J (2007) Subannual, seasonal, and interannual variability of the north Atlantic meridional overturning circulation. *J Phys Oceanogr* 37:1246–1265. <https://doi.org/10.1175/JPO3049.1>
- Jackson LC, de Asenjo EA, Bellomo K, Danabasoglu G, Haak H, Hu A, Jungclaus J, Lee W, Meccia VL, Saenko O, Shao A, Swingedouw D (2022) Understanding AMOC stability: the north Atlantic hosing model intercomparison project. <https://doi.org/10.5194/gmd-2022-277>
- Jackson LC, Kahana R, Graham T, Ringer MA, Woollings T, Mecking JV, Wood RA (2015) Global and European climate impacts of a slowdown of the AMOC in a high resolution GCM. *Clim Dyn* 45(11–12):3299–3316. <https://doi.org/10.1007/s00382-015-2540-2>
- Jackson L, Smith RS, Wood R (2016) Ocean and atmosphere feedbacks affecting AMOC hysteresis in a GCM. *Clim Dyn* 49:173–191. <https://doi.org/10.1007/s00382-016-3336-8>
- Jayne SR, Marotzke J (2001) The dynamics of ocean heat transport variability. *Rev Geophys* 39(3):385–411. <https://doi.org/10.1029/2000RG000084>
- Johnson HL, Cessi P, Marshall DP, Schloesser F, Spall MA (2019) Recent contributions of theory to our understanding of the Atlantic meridional overturning circulation. *J Geophys Res Oceans* 124(8):5376–5399. <https://doi.org/10.1029/2019jc015130>
- Jungclaus JH, Lorenz SJ, Schmidt H, Brovkin V, Brüggemann N, Chegini F, Crüger T, De-Vrese P, Gayler V, Giorgetta MA, Gutjahr O, Haak H, Hagemann S, Hanke M, Ilyina T, Korn P, Kröger J, Linardakis L, Mehlmann C, Mikolajewicz U, Müller WA, Nabel JEMS, Notz D, Pohlmann H, Putrasahan DA, Raddatz T, Ramme L, Redler R, Reick CH, Riddick T, Sam T, Schneek R, Schnur R, Schupfner M, Storch J-S, Wachsmann F, Wieners K-H, Ziemann F, Stevens B, Marotzke J, Claussen M (2022) The ICON earth system model version 1.0. *J Adv Model Earth Syst.* <https://doi.org/10.1029/2021ms002813>
- Kanzow T, Cunningham SA, Johns WE, Hirschi JJ-M, Marotzke J, Baringer MO, Meinen CS, Chidichimo MP, Atkinson C, Beal LM, Bryden HL, Collins J (2010) Seasonal variability of the Atlantic meridional overturning circulation at 26.5°N. *J Clim* 23(21):5678–5698. <https://doi.org/10.1175/2010JCLI3389.1>
- Knight JR (2005) A signature of persistent natural thermohaline circulation cycles in observed climate. *Geophys Res Lett.* <https://doi.org/10.1029/2005GL024233>
- Knutti R, Flückiger J, Stocker TF, Timmermann A (2004) Strong hemispheric coupling of glacial climate through freshwater discharge and ocean circulation. *Nature* 430(7002):851–856. <https://doi.org/10.1038/nature02786>
- Kuhlbrodt T, Griesel A, Montoya M, Levermann A, Hofmann M, Rahmstorf S (2007) On the driving processes of the Atlantic meridional overturning circulation. *Rev Geophys.* <https://doi.org/10.1029/2004RG000166>
- Kuhlbrodt T, Jones CG, Sellar A, Storkey D, Blockley E, Stringer M, Hill R, Graham T, Ridley J, Blaker A, Calvert D, Copey D, Ellis R, Hewitt H, Hyder P, Ineson S, Mulcahy J, Sahaan A, Walton J (2018) The low-resolution version of HadGEM3 GC3.1: development and evaluation for global climate. *J Adv Model Earth Syst* 10(11):2865–2888. <https://doi.org/10.1029/2018ms001370>
- LaCasce JH, Isachsen PE (2010) The linear models of the ACC. *Prog Oceanogr* 84:139–157. <https://doi.org/10.1016/j.pocean.2009.11.002>
- Levang SJ, Schmitt RW (2020a) What causes the AMOC to weaken in CMIP5? *J Clim* 33(4):1535–1545. <https://doi.org/10.1175/JCLI-D-19-0547.1>
- Levang SJ, Schmitt J (2020b) Intergyre salt transport in the climate warming response. *J Phys Oceanogr* 50(1):255–268. <https://doi.org/10.1175/jpo-d-19-0166.1>
- Li F, Lozier MS, Bacon S, Bower AS, Cunningham SA, de Jong MF, deYoung B, Fraser N, Fried N, Han G, Holliday NP, Holte J, Houpert L, Inall ME, Johns WE, Jones S, Johnson C, Karstensen J, Le Bras IA, Lherminier P, Lin X, Mercier H, Oltmanns M, Pacini A, Petit T, Pickart RS, Rayner D, Straneo F, Thierry V, Visbeck M, Yashayaev I, Zhou C (2021) Subpolar north Atlantic western boundary density anomalies and the meridional overturning circulation. *Nat Commun* 12(1):3002. <https://doi.org/10.1038/s41467-021-23350-2>
- Li L, Lozier MS, Li F (2022) Century-long cooling trend in subpolar north Atlantic forced by atmosphere: an alternative explanation. *Clim Dyn* 58(9–10):2249–2267. <https://doi.org/10.1007/s00382-021-06003-4>
- Lin WY, Zhang MH (2004) Evaluation of clouds and their radiative effects simulated by the NCAR community atmospheric model against satellite observations. *J Clim* 17(17):3302–3318. [https://doi.org/10.1175/1520-0442\(2004\)017<3302:EOCATR>2.0.CO;2](https://doi.org/10.1175/1520-0442(2004)017<3302:EOCATR>2.0.CO;2)
- Liu W, Liu Z, Brady EC (2014) Why is the AMOC monostable in coupled general circulation models? *J Clim* 27(6):2427–2443. <https://doi.org/10.1175/JCLI-D-13-00264.1>
- Liu W, Xie S-P, Liu Z, Zhu J (2017) Overlooked possibility of a collapsed Atlantic meridional overturning circulation in warming climate. *Sci Adv* 3:1601666. <https://doi.org/10.1126/sciadv.1601666>
- Liu W, Fedorov A, Sévellec F (2019) The mechanisms of the Atlantic meridional overturning circulation slowdown induced by arctic sea ice decline. *J Clim* 32(4):977–996. <https://doi.org/10.1175/JCLI-D-18-0231.1>
- Liu W, Fedorov AV, Xie SP, Hu S (2020) Climate impacts of a weakened Atlantic meridional overturning circulation in a warming climate. *Sci Adv.* <https://doi.org/10.1126/sciadv.aaz4876>
- Lopez H, Dong S, Lee S-K, Goni G (2016) Decadal modulations of interhemispheric global atmospheric circulations and monsoons by the south Atlantic meridional overturning circulation. *J Clim* 29(5):1831–1851. <https://doi.org/10.1175/JCLI-D-15-0491.1>
- Lovato T, Peano D, Butenschön M, Materia S, Iovino D, Scoccimarro E, Fogli PG, Cherchi A, Bellucci A, Gualdi S, Masina S, Navarra A (2022) CMIP6 simulations with the CMCC earth system model (CMCC-ESM2). *J Adv Model Earth Syst.* <https://doi.org/10.1029/2021ms002814>
- Lozier MS, Bacon S, Bower AS, Cunningham SA, De Jong MF, De Steur L, Deyoung B, Fischer J, Gary SF, Greenan BJ et al (2017) Overturning in the subpolar north Atlantic program: a new international ocean observing system. *Bull Am Meteorol Soc* 98(4):737–752. <https://doi.org/10.1175/BAMS-D-16-0057.1>
- Lozier MS, Li F, Bacon S, Bahr F, Bower AS, Cunningham SA, de Jong MF, de Steur L, deYoung B, Fischer J, Gary SF, Greenan BJW, Holliday NP, Houk A, Houpert L, Inall ME, Johns WE, Johnson HL, Johnson C, Karstensen J, Koman G, Bras IAL, Lin X, Mackay N, Marshall DP, Mercier H, Oltmanns M, Pickart RS, Ramsey AL, Rayner D, Straneo F, Thierry V, Torres DJ, Williams RG, Wilson C, Yang J, Yashayaev I, Zhao J (2019) A sea change in our view of overturning in the subpolar north Atlantic. *Science* 363(6426):516–521. <https://doi.org/10.1126/science.aau6592>
- Ma X, Liu W, Allen RJ, Huang G, Li X (2020) Dependence of regional ocean heat uptake on anthropogenic warming scenarios. *Sci Adv.* <https://doi.org/10.1126/sciadv.abc0303>
- Manabe S, Stouffer RJ (1995) Simulation of abrupt climate change induced by freshwater input to the north Atlantic ocean. *Nature* 378(6553):165–167. <https://doi.org/10.1038/378165a0>

- Maroon E, Kay J, Karnauskas K (2018) Influence of the Atlantic meridional overturning circulation on the northern hemisphere surface temperature response to radiative forcing. *J Clim* 31:9207–9224. <https://doi.org/10.1175/JCLI-D-17-0900.1>
- Mauritsen T, Bader J, Becker T, Behrens J, Bittner M, Brokopf R, Brovkin V, Claussen M, Crueger T, Esch M, Fast I, Fiedler S, Fläschner D, Gayler V, Giorgetta M, Goll DS, Haak H, Hagemann S, Hedemann C, Hohenegger C, Ilyina T, Jahns T, Jimenez-de-la-Cuesta D, Jungclaus J, Kleinen T, Kloster S, Kracher D, Kinne S, Kleberg D, Lasslop G, Kornbluh L, Marotzke J, Matei D, Meraner K, Mikolajewicz U, Modali K, Möbis B, Müller WA, Nabel JEMS, Nam CCW, Notz D, Nyawira S-S, Paulsen H, Peters K, Pincus R, Pohlmann H, Pongratz J, Popp M, Raddatz TJ, Rast S, Redler R, Reick CH, Rohrschneider T, Schemann V, Schmidt H, Schnur R, Schulzweida U, Six KD, Stein L, Stemmler I, Stevens B, Storch J-S, Tian F, Voigt A, Vrese P, Wieners K-H, Wilkenskeld S, Winkler A, Roeckner E (2019) Developments in the MPI-m earth system model version 1.2 (MPI-ESM1.2) and its response to increasing CO₂. *J Adv Model Earth Syst* 11(4):998–1038. <https://doi.org/10.1029/2018ms001400>
- Mauritzen C (1996) Production of dense overflow waters feeding the north Atlantic across the Greenland–Scotland ridge. Part 1: evidence for a revised circulation scheme. *Deep Sea Res Part I* 43(6):769–806. [https://doi.org/10.1016/0967-0637\(96\)00037-4](https://doi.org/10.1016/0967-0637(96)00037-4)
- McCarthy G, Frajka-Williams E, Johns WE, Baringer MO, Meinen CS, Bryden H, Rayner D, Duchez A, Roberts C, Cunningham SA (2012) Observed interannual variability of the Atlantic meridional overturning circulation at 26.5°N. *Geophys Res Lett*. <https://doi.org/10.1029/2012GL052933>
- Mecking J, Drijfhout S, Jackson L, Graham T (2016) Stable AMOC off state in an eddy-permitting coupled climate model. *Clim Dyn* 47:2455–2470. <https://doi.org/10.1007/s00382-016-2975-0>
- Menary MB, Robson J, Allan RP, Booth BBB, Cassou C, Gastineau G, Gregory J, Hodson D, Jones C, Mignot J, Ringer M, Sutton R, Wilcox L, Zhang R (2020) Aerosol-forced AMOC changes in CMIP6 historical simulations. *Geophys Res Lett* 47(14):2020–088166. <https://doi.org/10.1029/2020GL088166>
- Müller WA, Jungclaus JH, Mauritsen T, Baehr J, Bittner M, Budich R, Bunzel F, Esch M, Ghosh R, Haak H, Ilyina T, Kleine T, Kornbluh L, Li H, Modali K, Notz D, Pohlmann H, Roeckner E, Stemmler I, Tian F, Marotzke J (2018) A higher-resolution version of the Max Planck Institute Earth System Model (MPI-ESM1.2-HR). *J Adv Model Earth Syst* 10(7):1383–1413. <https://doi.org/10.1029/2017ms001217>
- Neubauer D, Ferrachat S, Drian CS-L, Stier P, Partridge DG, Tegen I, Bey I, Stanelle T, Kokkola H, Lohmann U (2019) The global aerosol-climate model ECHAM6.3–HAM2.3—part 2: cloud evaluation, aerosol radiative forcing, and climate sensitivity. *Geosci Model Dev* 12(8):3609–3639. <https://doi.org/10.5194/gmd-12-3609-2019>
- Nycander J, Nilsson J, Döös K, Broström G (2007) Thermodynamic analysis of ocean circulation. *J Phys Oceanogr* 37(8):2038–2052. <https://doi.org/10.1175/JPO3113.1>
- Park S, Shin J, Kim S, Oh E, Kim Y (2019) Global climate simulated by the Seoul National University atmosphere model version 0 with a unified convection scheme (SAM0-UNICON). *J Clim* 32(10):2917–2949. <https://doi.org/10.1175/jcli-d-18-0796.1>
- Polo I, Robson J, Sutton R, Balmaseda MA (2014) The importance of wind and buoyancy forcing for the boundary density variations and the geostrophic component of the AMOC at 26°N. *J Phys Oceanogr* 44:2387–2408. <https://doi.org/10.1175/JPO-D-13-0264.1>
- Proshutinsky A, Dukhovskoy D, Timmermans M-L, Krishfield R, Bamber JL (2015) Arctic circulation regimes. *Philos Trans A Math Phys Eng Sci* 373(2052):20140160. <https://doi.org/10.1098/rsta.2014.0160>
- Rahmstorf S, Box JE, Feulner G, Mann ME, Robinson A, Rutherford S, Schaffernicht EJ (2015) Exceptional twentieth-century slowdown in Atlantic ocean overturning circulation. *Nat Climate Change* 5:475–480. <https://doi.org/10.1038/nclimate2554>
- Reintges A, Martin T, Latif M, Keenlyside NS (2017) Uncertainty in twenty-first century projections of the Atlantic meridional overturning circulation in CMIP3 and CMIP5 models. *Clim Dyn* 49(5–6):1495–1511. <https://doi.org/10.1007/s00382-016-3180-x>
- Rind D, deMenocal P, Russell G, Sheth S, Collins D, Schmidt G, Teller J (2001) Effects of glacial meltwater in the GISS coupled atmosphere ocean model: 1. North Atlantic deep water response. *J Geophys Res* 106(D21):27335–27353. <https://doi.org/10.1029/2000JD000070>
- Rind D, Orbe C, Jonas J, Nazarenko L, Zhou T, Kelley M, Lacis A, Shindell D, Faluvegi G, Romanou A, Russell G, Tausnev N, Bauer M, Schmidt G (2020) GISS model e2.2: a climate model optimized for the middle atmosphere-model structure, climatology, variability, and climate sensitivity. *J Geophys Res Atmos*. <https://doi.org/10.1029/2019jd032204>
- Robson J, Hodson D, Hawkins E, Sutton R (2013) Atlantic overturning in decline? *Nat Geosci* 7(1):2–3. <https://doi.org/10.1038/ngeo2050>
- Schmidt GA, Kelley M, Nazarenko L, Ruedy R, Russell GL, Aleinov I, Bauer M, Bauer SE, Bhat MK, Bleck R, Canuto V, Chen Y-H, Cheng Y, Clune TL, Genio AD, de Fainchtein R, Faluvegi G, Hansen JE, Healy RJ, Kiang NY, Koch D, Lacis AA, LeGrande AN, Lerner J, Lo KK, Matthews EE, Menon S, Miller RL, Oinas V, Olosio AO, Perlwitz JP, Puma MJ, Putman WM, Rind D, Romanou A, Sato M, Shindell DT, Sun S, Syed RA, Tausnev N, Tsigaridis K, Unger N, Voulgarakis A, Yao M-S, Zhang J (2014) Configuration and assessment of the GISS ModelE2 contributions to the CMIP5 archive. *J Adv Model Earth Syst* 6(1):141–184. <https://doi.org/10.1002/2013ms000265>
- Schmittner A, Latif M, Schneider B (2005) Model projections of the north Atlantic thermohaline circulation for the 21st century assessed by observations. *Geophys Res Lett*. <https://doi.org/10.1029/2005GL024368>
- Schmitz Jr WJ (1996) On the world ocean circulation. Volume 1. Some global features/north Atlantic circulation. Technical Report, Woods Hole Oceanographic Institution, MA. <https://doi.org/10.1575/1912/355>
- Séférian R, Nabat P, Michou M, Saint-Martin D, Voltaire A, Colin J, Decharme B, Delire C, Berthet S, Chevallier M, Sénési S, Franchisteguy L, Vial J, Mallet M, Joetzjer E, Geoffroy O, Guérémy J-F, Moine M-P, Msadek R, Ribes A, Rocher M, Roehrig R, Salas-y-Méllia D, Sanchez E, Terray L, Valcke S, Waldman R, Aumont O, Bopp L, Deshayes J, Été C, Madec G (2019) Evaluation of CNRM earth system model, CNRM-ESM2-1: role of earth system processes in present-day and future climate. *J Adv Model Earth Syst* 11(12):4182–4227. <https://doi.org/10.1029/2019ms001791>
- Seland Ø, Bentsen M, Olivie D, Toniazzo T, Gjermundsen A, Graff LS, Debernard JB, Gupta AK, He Y-C, Kirkevåg A, Schwinger J, Tjiputra J, Aas KS, Bethke I, Fan Y, Griesfeller J, Grini A, Guo C, Ilicak M, Karset IHH, Landgren O, Liakka J, Moseid KO, Nummelin A, Spensberger C, Tang H, Zhang Z, Heinze C, Iversen T, Schulz M (2020) Overview of the Norwegian earth system model (NORESM2) and key climate response of cmip6 deck, historical, and scenario simulations. *Geosci Model Dev* 13(12):6165–6200. <https://doi.org/10.5194/gmd-13-6165-2020>
- Sellar AA, Jones CG, Mulcahy JP, Tang Y, Yool A, Wiltshire A, O'Connor FM, Stringer M, Hill R, Palmieri J, Woodward S, Mora L, Kuhlbrodt T, Rumbold ST, Kelley DI, Ellis R,

- Johnson CE, Walton J, Abraham NL, Andrews MB, Andrews T, Archibald AT, Berthou S, Burke E, Blockley E, Carslaw K, Dalvi M, Edwards J, Folberth GA, Gedney N, Griffiths PT, Harper AB, Hendry MA, Hewitt AJ, Johnson B, Jones A, Jones CD, Keeble J, Liddicoat S, Morgenstern O, Parker RJ, Predoi V, Robertson E, Siahhaan A, Smith RS, Swaminathan R, Woodhouse MT, Zeng G, Zerroukat M (2019) UKESM1: description and evaluation of the U.K. earth system model. *J Adv Model Earth Syst* 11(12):4513–4558. <https://doi.org/10.1029/2019ms001739>
- Smeed DA (2014) Observed decline of the Atlantic meridional overturning circulation 2004–2012. *Ocean Sci* 10:29–38. <https://doi.org/10.5194/os-10-29-2014>
- Smeed DA (2018) The north Atlantic ocean is in a state of reduced overturning. *Geophys Res Lett* 45:1527–1533. <https://doi.org/10.1002/2017GL076350>
- Spall MA, Pickart RS (2001) Where does dense water sink? A subpolar gyre example. *J Phys Oceanogr* 31(3):810–826. [https://doi.org/10.1175/1520-0485\(2001\)031<0810:WDDWSA>2.0.CO;2](https://doi.org/10.1175/1520-0485(2001)031<0810:WDDWSA>2.0.CO;2)
- Stocker TF, Johnsen SJ (2003) A minimum thermodynamic model for the bipolar seesaw. *Paleoceanography*. <https://doi.org/10.1029/2003PA000920>
- Stommel H (1961) Thermohaline convection with two stable regimes of flow. *Tellus B*. <https://doi.org/10.3402/tellusa.v13i2.9491>
- Stommel H, Arons AB (1959) On the abyssal circulation of the world ocean-i. Stationary planetary flow patterns on a sphere. *Deep Sea Res* (1953) 6:140–154. [https://doi.org/10.1016/0146-6313\(59\)90065-6](https://doi.org/10.1016/0146-6313(59)90065-6)
- Stouffer R, Yin J-J, Gregory J, Dixon K, Spelman M, Hurlin W, Weaver A, Eby M, Flato G, Hasumi H, Hu A, Jungclaus J, Kamenkovich I, Levermann A, Montoya M, Murakami S, Nawrath S, Oka A, Peltier W, Robitaille DY, Sokolov A, Vettoretti G, Weber S (2006) Investigating the causes of the response of the thermohaline circulation to past and future climate changes. *J Clim* 19:1365–1387. <https://doi.org/10.1175/JCLI3689.1>
- Swart NC, Cole JNS, Kharin VV, Lazare M, Scinocca JF, Gillett NP, Anstey J, Arora V, Christian JR, Hanna S, Jiao Y, Lee WG, Majaess F, Saenko OA, Seiler C, Seinen C, Shao A, Sigmond M, Solheim L, von Salzen K, Yang D, Winter B (2019) The Canadian earth system model version 5 (CanESM5.0.3). *Geosci Model Dev* 12(11):4823–4873. <https://doi.org/10.5194/gmd-12-4823-2019>
- Tatebe H, Ogura T, Nitta T, Komuro Y, Ogochi K, Takemura T, Sudo K, Sekiguchi M, Abe M, Saito F, Chikira M, Watanabe S, Mori M, Hirota N, Kawatani Y, Mochizuki T, Yoshimura K, Takata K, O'ishi R, Yamazaki D, Suzuki T, Kurogi M, Kataoka T, Watanabe M, Kimoto M (2019) Description and basic evaluation of simulated mean state, internal variability, and climate sensitivity in MIROC6. *Geosci Model Dev* 12(7):2727–2765. <https://doi.org/10.5194/gmd-12-2727-2019>
- Tegen I, Neubauer D, Ferrachat S, Drian CS-L, Bey I, Schutgens N, Stier P, Watson-Parris D, Stanelle T, Schmidt H, Rast S, Kokkola H, Schultz M, Schroeder S, Daskalakis N, Barthel S, Heinold B, Lohmann U (2019) The global aerosol-climate model ECHAM6.3-HAM2.3—part 1: aerosol evaluation. *Geosci Model Dev* 12(4):1643–1677. <https://doi.org/10.5194/gmd-12-1643-2019>
- Toggweiler JR, Samuels B (1995) Effect of drake passage on the global thermohaline circulation. *Deep Sea Res Part I* 42(4):477–500. [https://doi.org/10.1016/0967-0637\(95\)00012-U](https://doi.org/10.1016/0967-0637(95)00012-U)
- Toggweiler JR, Samuels B (1998) On the ocean's large-scale circulation near the limit of no vertical mixing. *J Phys Oceanogr* 28(9):1832–1852. [https://doi.org/10.1175/1520-0485\(1998\)028<1832:OTOSLS>2.0.CO;2](https://doi.org/10.1175/1520-0485(1998)028<1832:OTOSLS>2.0.CO;2)
- Trenberth KE, Caron JM, Stepaniak DP (2001) The atmospheric energy budget and implications for surface fluxes and ocean heat transports. *Clim Dyn* 17(4):259–276. <https://doi.org/10.1007/pl00007927>
- Vellinga M, Wood R (2002) Global climatic impacts of a collapse of the Atlantic thermohaline circulation. *Clim Change* 54:251–267. <https://doi.org/10.1023/A:1016168827653>
- Visbeck M (2007) Power of pull. *Nature* 447(7143):383–383. <https://doi.org/10.1038/447383a>
- Voldoire A, Saint-Martin D, Sénési S, Decharme B, Alias A, Chevalier M, Colin J, Guérémy J-F, Michou M, Moine M-P, Nabat P, Roebrig R, Méliá DS, Sférian R, Valcke S, Beau I, Belamari S, Berthet S, Cassou C, Cattiaux J, Deshayes J, Douville H, Ethé C, Franchistéguy L, Geoffroy O, Lévy C, Madec G, Meurdesoif Y, Msadek R, Ribes A, Sanchez-Gomez E, Terray L, Waldman R (2019) Evaluation of CMIP6 DECK experiments with CNRM-CM6-1. *J Adv Model Earth Syst* 11(7):2177–2213. <https://doi.org/10.1029/2019ms001683>
- Volodin EM, Mortikov EV, Kostykin SV, Galin VY, Lykossov VN, Gritsun AS, Diansky NA, Gusev AV, Iakovlev NG (2017) Simulation of the present-day climate with the climate model INMCM5. *Clim Dyn* 49(11–12):3715–3734. <https://doi.org/10.1007/s00382-017-3539-7>
- Volodin EM, Mortikov EV, Kostykin SV, Galin VY, Lykossov VN, Gritsun AS, Diansky NA, Gusev AV, Iakovlev NG, Shestakova AA, Emelina SV (2018) Simulation of the modern climate using the INM-CM48 climate model. *Russ J Numer Anal Math Model* 33(6):367–374. <https://doi.org/10.1515/rnam-2018-0032>
- Weaver AJ, Eby M, Kienast M, Saenko OA (2007) Response of the Atlantic meridional overturning circulation to increasing atmospheric CO₂: sensitivity to mean climate state. *Geophys Res Lett*. <https://doi.org/10.1029/2006GL028756>
- Weaver AJ, Sedláček J, Eby M, Alexander K, Crespin E, Fichet T, Philippon-Berthier G, Joos F, Kawamiya M, Matsumoto K, Steinacher M, Tachiiri K, Tokos K, Yoshimori M, Zickfeld K (2012) Stability of the Atlantic meridional overturning circulation: a model intercomparison. *Geophys Res Lett*. <https://doi.org/10.1029/2012GL053763>
- Weijer W, Cheng W, Drijfhout SS, Fedorov AV, Hu A, Jackson LC, Liu W, McDonagh EL, Mecking JV, Zhang J (2019) Stability of the Atlantic meridional overturning circulation: a review and synthesis. *J Geophys Res Oceans* 124(8):5336–5375. <https://doi.org/10.1029/2019JC015083>
- Weijer W, Cheng W, Garuba OA, Hu A, Nadiga BT (2020) CMIP6 models predict significant 21st century decline of the Atlantic meridional overturning circulation. *Geophys Res Lett*. <https://doi.org/10.1029/2019GL086075>
- Weijer W, Haine T, Siddiqui A, Cheng W, Veneziani M, Kurtakoti P (2022) Interactions between the Arctic Mediterranean and the Atlantic meridional overturning circulation: a review. *Oceanography*. <https://doi.org/10.5670/oceanog.2022.130>
- Williams KD, Copey D, Blockley EW, Bodas-Salcedo A, Calvert D, Comer R, Davis P, Graham T, Hewitt HT, Hill R, Hyder P, Ineson S, Johns TC, Keen AB, Lee RW, Megann A, Milton SF, Rae JGL, Roberts MJ, Scaife AA, Schiemann R, Storkey D, Thorpe L, Watterson IG, Walters DN, West A, Wood RA, Woollings T, Xavier PK (2018) The met office global coupled model 3.0 and 3.1 (GC3.0 and GC3.1) configurations. *J Adv Model Earth Syst* 10(2):357–380. <https://doi.org/10.1002/2017ms001115>
- Wright DG, Stocker TF (1991) A zonally averaged ocean model for the thermohaline circulation. Part i: model development and flow dynamics. *J Phys Oceanogr* 21(12):1713–1724. [https://doi.org/10.1175/1520-0485\(1991\)021<1713:AZAOMF>2.0.CO;2](https://doi.org/10.1175/1520-0485(1991)021<1713:AZAOMF>2.0.CO;2)
- Wunsch C (2002) What is the thermohaline circulation? *Science* 298:1179–1181. <https://doi.org/10.1126/science.1079329>

- Wunsch C (2004) Vertical mixing, energy, and the general circulation of the oceans. *Annu Rev Fluid Mech* 36(1):281–314. <https://doi.org/10.1146/annurev.fluid.36.050802.122121>
- Yeager S (2015) Topographic coupling of the Atlantic overturning and gyre circulations. *J Phys Oceanogr* 45(5):1258–1284. <https://doi.org/10.1175/JPO-D-14-0100.1>
- Yeager S, Danabasoglu G (2014) The origins of late-twentieth-century variations in the large-scale north Atlantic circulation. *J Clim* 27(9):3222–3247. <https://doi.org/10.1175/JCLI-D-13-00125.1>
- Yukimoto S, Kawai H, Koshiro T, Oshima N, Yoshida K, Urakawa S, Tsujino H, Deushi M, Tanaka T, Hosaka M, Yabu S, Yoshimura H, Shindo E, Mizuta R, Obata A, Adachi Y, Ishii M (2019) The meteorological research institute earth system model version 2.0, MRI-ESM2.0: description and basic evaluation of the physical component. *J Meteorol Soc Jpn Ser II* 97(5):931–965. <https://doi.org/10.2151/jmsj.2019-051>
- Zhang R, Sutton R, Danabasoglu G, Kwon Y-O, Marsh R, Yeager SG, Amrhein DE, Little CM (2019) A review of the role of the Atlantic meridional overturning circulation in Atlantic multidecadal variability and associated climate impacts. *Rev Geophys* 57(2):316–375. <https://doi.org/10.1029/2019RG000644>
- Ziehn T, Chamberlain MA, Law RM, Lenton A, Bodman RW, Dix M, Stevens L, Wang Y-P, Srbinovsky J (2020) The Australian earth system model: ACCESS-ESM1.5. *J South Hemisphere Earth Syst Sci* 70(1):193. <https://doi.org/10.1071/es19035>

Publisher's Note Springer Nature remains neutral with regard to jurisdictional claims in published maps and institutional affiliations.